THE ASTRONOMICAL JOURNAL VOLUME 106, NUMBER 2 AUGUST 1993

STAR FORMATION IN EARLY-TYPE GALAXIES IN THE COMA CLUSTER

NELSON CALDWELL[1]
F. L. Whipple Observatory, Smithsonian Institution, P.O. Box 97, Amado, Arizona 85645
Electronic mail: caldwell@flwo99.sao.arizona.edu

JAMES A. ROSE[1]
Department of Physics and Astronomy, University of North Carolina, Chapel Hill, North Carolina 27599
Electronic mail: jim@wrath.physics.edu

RAY M. SHARPLES[1] AND RICHARD S. ELLIS
Department of Physics, University of Durham, Durham DH1 3LE, United Kingdom
Electronic mail: rsharples@starlink.durham.ac.uk, rse@starlink.durham.ac.uk

RICHARD G. BOWER
Max-Planck-Institut fur Extraterrestrische Physik, Giessenbachstrasse, D-8046 Garching bei Munchen, Germany
Electronic mail: rgb@mpeu19.mpe-garching.mpg.de

Received 1993 February 3; revised 1993 April 14

ABSTRACT

We have obtained multifiber spectra of 125 early-type galaxies in the Coma cluster of galaxies, using the Hydra bench spectrograph on the 4 m telescope at Kitt Peak. The sample selection was based on both color and morphology, care being taken to exclude intermediate and late-type spirals. Surprisingly, a large fraction (about 1/3) of all galaxies in a field located approximately 40′ SW of the center of the cluster exhibits enhanced Balmer absorption lines or emission lines, indicative of recent star formation or nuclear activity. In contrast, very few such galaxies are found in the central field of the cluster. Those galaxies with abnormal spectra cover a range in luminosity down to $B \approx 19$ ($M_B \approx -15$). Furthermore, the bulk of the abnormal-spectrum galaxies are located near a secondary peak in the cluster x-ray emission found by Briel *et al.* [A&A, 259, L31 (1992)] and by Watt *et al.* [MNRAS, 258, 738 (1992)]. We argue by detailed comparisons with Kennicutt's [ApJS, 79, 255 (1992a)] sequence of normal spiral galaxy spectra that the anomalous spectral features cannot arise from morphological misindentifications. Specifically, the abnormal spectra are fundamentally different, with [O II] emission lines too weak for the enhanced Balmer absorption. The spectra are, however, remarkably similar to the red Hδ-strong galaxies studied by Couch & Sharples [MNRAS, 229, 423 (1987)] in clusters at redshift $z \approx 0.3$ Hence it appears that an environmental process similar to that frequently found in clusters at moderate redshift is occurring at the present epoch in the outskirts of the Coma cluster.

1. INTRODUCTION

Detailed studies of moderate redshift clusters (Butcher & Oemler 1978, 1984; Dressler & Gunn 1983; Couch & Sharples 1987) have revealed that a subset of the member galaxies show spectral features indicative of enhanced star formation, in contrast to the properties of their counterparts in the cores of similar present day clusters. This activity, referred to as the "Butcher–Oemler effect," manifests itself in a variety of ways in individual galaxies. Some galaxies are witnessed during an intense burst of star formation while others are viewed shortly after completing such a phase (the post-starburst or "E+A" galaxies). A major outstanding puzzle is the physical origin of the Butcher–Oemler effect. While several possible explanations have been proposed (cf. Oemler 1992), the great distances of the clusters exhibiting the effect has to date prevented a definitive answer from being obtained. Specifically, the faintness of the galaxies and the problems of field contamination in these distant clusters have severely hampered work on this subject. Traditionally, a comparison cluster at low redshift has been the Coma cluster, whose central galaxies (mostly S0's by number, with a 20% fraction of E's) do indeed appear bereft of recent star formation. The surprising result of this paper is that a large percentage of Coma galaxies in a field 40′ southwest of the cluster center have spectra similar to the abnormal galaxies in the more distant clusters. If the two effects are indeed related, in view of the relative proximity of the Coma cluster, our result may provide a breakthrough in studying the origin of the Butcher–Oemler effect.

Our original interest in studying the Coma cluster arose because of evidence that early-type galaxies have star-formation histories which depend on their environment. Bower *et al.* (1990) have shown that the Sr II, Fe I, and Hδ lines can be used to detect subtle stellar population

[1]Visiting Astronomer, Kitt Peak National Observatory, NOAO, which is operated by AURA, Inc., under contract with the National Science Foundation.

 0004-6256/93/106(2)/473/20/$0.90

differences in E/S0 galaxies. In particular, they report differences in certain spectral line ratios between E/S0 galaxies in dense clusters and those found in lower density environments, and further argue that such evidence indicates an older and more metal-poor stellar population in cluster galaxies. We thus hoped to find similar evidence for this effect in the detailed analysis of spectra of E/S0's in the inner and outer parts of the Coma cluster. As it turned out, even a visual inspection of the spectra was sufficient to show that *large* differences exist in the stellar populations of the two environments.

A plan of the paper follows. In Sec. 2 we summarize the multifiber observations of 125 galaxies in Coma obtained in this study. In Sec. 3 we demonstrate that a large fraction of galaxies in the SW region exhibits evidence of enhanced levels of recent star formation. Furthermore, we show that the abnormal spectra are unlike those of low-redshift star-forming galaxies, but are very similar to those of star-forming galaxies in intermediate-redshift clusters studied by Couch & Sharples (1987). We also discuss the relationship between the abnormal-spectrum galaxies in the SW region of Coma and the recently discovered secondary peak in x-ray emission found in approximately the same region by Briel *et al.* (1992) and by Watt *et al.* (1992). We summarize our conclusions in Sec. 4.

2. OBSERVATIONAL DATA

The prospect of using the KPNO multifiber positioner, called Hydra, with its 97 fibers and 45′ field meant that we would be able to observe more than 100 Coma galaxies for this study. Our sample of galaxies was thus selected from the extensive catalog of Godwin *et al.* (1983, hereafter referred to as GMP). This list is drawn from a 2.6 degree square field, centered on the cluster, and considered complete to $B=20$, corresponding to $M_B < -14$. In selecting early-type galaxies, we identified a subset of GMP galaxies using two criteria. First, we fitted the $(b-r,b)$ color-magnitude ridge line of the cluster early-type galaxies, and selected galaxies whose colors are within ± 0.15 mag of the relation. This method recovered most of the E/S0's classified by Dressler (1980a) but the list also includes many fainter unclassified galaxies and some galaxies of a type later than E/S0. The second criterion therefore involved independent morphological classifications into E, S0, E/S0, Sa, dE, etc., by one of us (N.C.), using KPNO 4 m prime focus plates where possible (70% of the sample), or glass copies of the Palomar Sky Survey.

In the overlap with Dressler, there was good agreement between the Dressler classifications and those based on the 4 m plates, giving us confidence in the classification of many faint galaxies not typed by Dressler. The color-selected list was thus trimmed of galaxies not classified as E, S0, or E/S0 on the 4 m plates. There proved to be a tendency for Dressler's early-type spirals to be classified as S0 on the 4 m plates, consequently some of these were included. A few galaxies (about 25 in number) that did not pass the color selection but which have clear E/S0 morphology were reinstated into the final list. Our final catalog

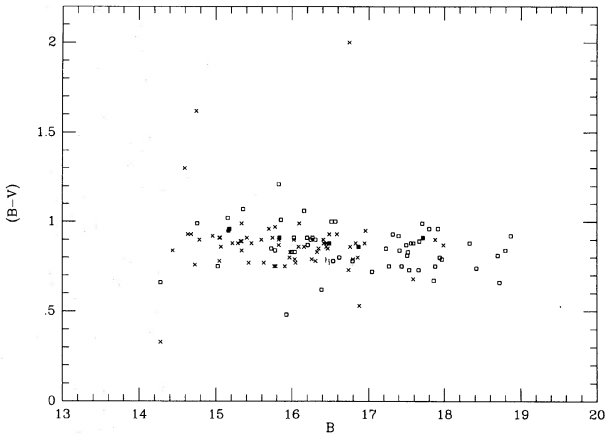

FIG. 1. $B-V$ vs B color–magnitude diagram for all Coma galaxies observed spectroscopically with Hydra. Crosses are for galaxies in the central field and squares are for galaxies in the SW field. Transformation of the GMP $b-r$ colors into $B-V$ colors was carried out using the relation $(B-V)=(b-r)-0.925$, obtained from a comparison of colors for galaxies in common between the GMP catalog and the compilation of Burstein *et al.* (1987). The B magnitudes have been left on the GMP system and, along with the colors, have been K-corrected. Galaxies deviating by more than 0.15 mag from the mean sequence were included in the sample on the basis that Dressler (1980a) classifies them as E or S0 (see discussion in Sec. 2). The dashed line indicates the apparent $B=17.2$ magnitude limit discussed in the text (also K-corrected here).

should thus be complete for early-type galaxies within the 2.6 square degrees surveyed by GMP. Finally, we removed all galaxies brighter than $B=14.3$, since galaxies with velocity dispersions greater than about 220 km s^{-1} would not be useful in the planned analyses of the weak absorption lines (see, Bower *et al.* 1990, for details). Our spectroscopic source list should thus be representative of those galaxies in the Coma cluster with uniformly old stellar populations.

Our catalog contains 590 galaxies, comprising 50% S0's, 17% E's, 27% E/S0's, and 6% other types/unclassified. For the Hydra run, we selected galaxies in two 45′ regions: one centered on the cluster core (which contained 134 galaxies total) and one centered 40′ SW of the cluster center (71 galaxies). The Hydra configuration program selected as many galaxies in a field as the proximity requirements of the fibers would allow, and remaining fibers were positioned to predetermined sky positions. This program worked through the list in order of brightness which, because of the lower surface density of galaxies in the SW region, resulted in a fainter magnitude distribution than for the central field. The range observed in the central field was $14.3 < B < 18.1$ as opposed to $14.3 < B < 19.0$ for the SW field (see Fig. 1).

All spectroscopic data were obtained with the Hydra multifiber positioner and bench spectrograph on the KPNO 4 m telescope in March 1992. The blue fiber cable was used in conjunction with a 316 lines mm^{-1} grating in second order to yield a dispersion of 1.0 Å pixel^{-1} and spectral resolution of 3.8 Å FWHM. A thinned, blue-sensitive Tektronix 2048^2 CCD (TK2B) was used as the detector. The number of spectra accessible simultaneously

with Hydra is sufficiently large that we decided to expose on one field per night, thus insuring spectra of much higher signal-to-noise ratio than typically obtained when galaxies are observed on an individual basis. A total of six 1 h exposures were obtained of the central field, through thin clouds. For the SW field, we obtained six 55 min exposures (total 5.5 h), through somewhat thicker clouds. The anticipated third night of observations was entirely clouded out. The individual frames were combined using a cosmic ray removal algorithm. During these nights, velocity and spectral standards were also observed, typically through only 1 fiber. As the nights were not photometric, no flux standards were observed. In order to get approximate emission-line flux ratios for the galaxies exhibiting emission-line spectra, we used the spectral energy distribution of the E galaxy NGC 3379, kindly provided to us by Kennicutt (see Kennicutt 1992a), to correct our Coma spectra onto a relative flux scale.

Dome and twilight flats, and HeNeAr exposures for wavelength calibration were also taken. The dome flats were not of sufficient signal to use in correcting pixel–pixel variations, which were minimal for the TK2B anyway, but were used to correct the relative throughput of the fibers, essential for accurate sky subtraction. The sky flats were used to define the locations of the spectra on the CCD, which were assumed to be the same for the cluster spectra. The IRAF program DOHYDRA was employed in the reduction in the following sequence: the spectra were (i) optimally extracted and cleaned for remaining cosmic rays, (ii) wavelength calibrated according to the HeNeAr spectrum taken through the same fiber, (iii) scaled according to the throughput correction and sky subtracted. The sky spectrum was typically a combination of ten individual sky spectra for each field, and was itself throughput corrected.

A total of 73 galaxy spectra were obtained in the central Coma field and 64 spectra in the SW field. Four of the SW spectra revealed these to be background galaxies; their properties are summarized in Appendix B. Furthermore, two of the SW spectra were of insufficient quality such that, although their velocities are consistent with cluster membership (where we consider a member to have a velocity $4500 < V < 10\,000$ km s^{-1}), no other reliable information could be extracted. A further galaxy classed as SBb by Dressler was removed from the SW sample, although its velocity is new and so we report it in the table. The SW and central fields overlapped slightly and there are five galaxies in common (D53, D69, D71, D72, and D91). Velocities and indices derived for these galaxies from both spectra agree within the errors. Because of the overlap, we had to reassign some galaxies to the other field, based on a boundary that seemed best to separate the galaxies into two groups (easily seen in Figs. 7 and 17). Of the galaxies in common, D53 was assigned to the SW field, the other four were assigned to the central field. D58 (originally observed in the central field) was reassigned to the SW field. D89, GMP 4420 and 4314 were reassigned from the SW to the central field. Consequently, in the discussion that follows we consider the spectra of 74 galaxies in the central field, and 51 galaxies in the SW field.

Basic data for all the galaxies observed are listed in Table 1. Column 1 is the fiber number, followed by a Dressler (1980a) catalog number where available, the GMP number, and an NGC/IC designation if one exists. Following the coordinates (equinox 2000) are the Dressler and NC classifications. A colon against NC's types indicates that Schmidt plates were used rather than KPNO 4m plates. The GMP magnitudes and colors are followed by the spectral signal level in counts per pixel (1 count = 13 CCD electrons) averaged over the whole spectrum; for reference, the mean sky count level over the spectrum is $\approx$20 counts per pixel. The remaining columns list the two spectroscopic line indices described below, whether the spectrum is abnormal (a check for a certain case, a colon for an uncertain case), and the heliocentric velocity of the galaxy with its error.

3. RESULTS

3.1 Analysis of Spectra

As expected, the overwhelming majority of the galaxies in the central field have spectra typical of an old stellar population, with no signs of recent star formation and/or nuclear activity. However, a large number of the galaxies in the SW field (about one-third of the sample) have spectral features indicative of recent star formation or nuclear activity; we refer to these as "abnormal spectra" leaving a precise definition until later. This is the main result of the paper, and in what follows we present quantitative evidence in support of unusual activity in the SW field. We then demonstrate that this activity does not simply reflect some residual radial segregation of morphological types (Melnick & Sargent 1977; Dressler 1980b; Whitmore & Gilmore 1991) that might have crept into our sample despite our careful selection criterion. Rather, the spectral abnormalities appear to be related to the evolutionary phenomenon observed in the environments of galaxy clusters at redshifts of $z \approx 0.3$–0.5.

The strength of our basic result can be readily demonstrated. Out of a total of 125 member galaxies in both fields, 15 have enhanced Balmer absorption lines indicative of recent star formation, 3 have AGN-like emission lines, and 2 have emission lines indicative of current star formation (17 in total, since some galaxies have both emission and Balmer absorption). There are a further 3 galaxies with weaker evidence of a similar nature. *All but 5 of these 20 galaxies are located in the SW field.* A qualitative impression of the types of activity found can be obtained from Fig. 2. In Fig. 2(a) are displayed those galaxies with both enhanced Balmer absorption lines as well as emission lines, whereas in Fig. 2(b) are plotted those systems with enhanced Balmer absorption and no detected emission. In Fig. 2(c) are displayed spectra dominated by AGN emission, while Fig. 2(d) shows a few normal galaxies with different luminosities.

In view of the higher proportion of faint galaxies observed in the SW field than in the central regions (see Sec.

TABLE 1. (a) Coma galaxies in the central field.

Spectrum	D	GMP	other	RA (2000)	Dec (2000)	Morph. D	Morph. C	b	b-r	Signal	CN/H8	Hδ (Å)	A?	$V_\odot$ (km s^{-1})
2	181	3972		12 58 50.6	28 5 2.3	S0	S0	16.52	1.87	197	0.41 ± 0.10	2.59 ± 0.25		6018 ± 11
3	174	2922	IC4012	13 0 7.8	28 4 42.7	E	E	15.93	1.86	399	0.38 ± 0.10	2.17 ± 0.18		7196 ± 15
4	57	3165		12 59 46.9	27 42 38.0	S0/a	S0	15.15	1.78	297	0.31 ± 0.09	2.73 ± 0.18		8342 ± 10
6	168	2440	IC4045	13 0 48.5	28 5 26.8	E	E	15.17	1.85	283	0.32 ± 0.08	1.63 ± 0.18		6896 ± 15
7	154	3291		12 59 38.1	27 59 13.2	S0	S0	16.41	1.78	93	−0.05 ± 0.13	2.10 ± 0.39		6812 ± 11
8	137	4315	NGC4850	12 58 21.7	27 58 4.0	E/S0	E/S0	15.39	1.87	372	−0.03 ± 0.09	2.16 ± 0.18		5994 ± 15
9		4083		12 58 40.7	27 49 37.8		S0	17.82	1.91	16	−1.61 ± 0.45			6202 ± 30
10		2478		13 0 45.3	27 50 8.0		S0	18.09	1.86	17	0.81 ± 0.37	2.00 ± 1.34		8720 ± 29
11	65	2945		13 0 6.1	27 46 30.8	S0	S0	16.15	1.77	97	0.73 ± 0.14	1.23 ± 0.36		6092 ± 12
12	122	2815	NGC4894	13 0 16.4	27 58 3.0	S0	S0	15.87	1.74	74	−0.43 ± 0.18	1.87 ± 0.39		4634 ± 10
13	176	3390		12 59 31.1	28 2 48.2	S0	S0	15.89	1.75	136	0.31 ± 0.11	2.39 ± 0.30		6832 ± 11
15	182	4200		12 58 31.8	28 2 58.5	S0	E	16.84	1.72	140	0.49 ± 0.09	2.38 ± 0.30		5705 ± 12
16	193	3084		12 59 54.9	28 7 41.8	E	E	16.43	1.82	168	0.57 ± 0.09	1.40 ± 0.28		7566 ± 12
17	171	2805		13 0 16.9	28 3 50.0	S0	S0	16.57	1.78	166	0.07 ± 0.09	1.89 ± 0.28		6141 ± 11
18	196	3935		12 58 53.3	28 7 33.6	E	S0	16.59	1.93	163	0.19 ± 0.13	1.90 ± 0.23		6976 ± 10
19	69	3730	IC3959	12 59 8.0	27 47 2.7	E	E	15.27	1.94	457	0.78 ± 0.08	2.29 ± 0.18		7053 ± 18
20	155	3367	NGC4873	12 59 32.5	27 59 0.2	S0	E/S0	15.15	1.91	312	0.63 ± 0.08	1.94 ± 0.18		5848 ± 13
21	88	3423	IC3976	12 59 29.2	27 51 0.4	S0	S0	15.80	1.95	400	0.69 ± 0.12	1.12 ± 0.18		6817 ± 20
22		2942		13 0 6.1	27 41 6.8		E	16.69	1.93	226	0.23 ± 0.08	2.00 ± 0.23		7537 ± 12
23	170	2727	IC4026	13 0 22.0	28 2 50.1	SB0	S0	15.73	1.77	59	0.35 ± 0.19	3.30 ± 0.51		8220 ± 13
24	206	2795	NGC4895	13 0 17.9	28 12 7.7	S0	S0	14.38	1.32	176	0.35 ± 0.09	1.97 ± 0.26		8488 ± 14
25	62	2393		13 0 53.8	27 47 0.7	S0	E/S0	16.51	1.90	159	0.25 ± 0.11	1.58 ± 0.28		8279 ± 10
29	119	2654		13 0 27.8	27 57 21.4	S0	S0	16.38	1.90	137	0.27 ± 0.12	1.87 ± 0.30		6984 ± 12
31	58	4017	NGC4854	12 58 47.2	27 40 29.0	S0	E	15.16	1.91	318	0.74 ± 0.12	1.97 ± 0.18		8364 ± 15
33	127	3254		12 59 40.2	27 58 6.3	S0	S0	16.57	1.84	36	−1.28 ± 0.19	1.10 ± 0.89	√	7514 ± 14
34	21¡8	3818		12 59 1.7	28 13 31.0	S0/a	S0	15.44	1.89	258	0.40 ± 0.06	2.05 ± 0.21		7972 ± 14
35	200	4379		12 58 14.9	28 7 33.1	S0	S0	16.08	1.82	241	0.36 ± 0.13	2.25 ± 0.21		7506 ± 13
36	78	2000	NGC4923	13 1 31.7	27 50 50.2	E	S0:	14.78	1.93	268	0.54 ± 0.15	1.69 ± 0.18		5409 ± 18
37	99	2897		13 0 10.1	27 51 49.6	S0	E/S0	16.98	1.53	77	−1.20 ± 0.16	4.51 ± 0.37	√	9902 ± 11
38	126	3206		12 59 44.0	27 57 30.3	S0	S0	16.36	1.79	171	0.24 ± 0.11	2.60 ± 0.28		6892 ± 9
40	208	3553		12 59 20.0	28 11 52.3	S0	S0	16.96	1.80	131	0.18 ± 0.13	2.75 ± 0.31		9439 ± 9
41	131	3414	NGC4871	12 59 29.8	27 57 21.2	S0	S0	14.89	1.90	171	0.53 ± 0.09	2.20 ± 0.29		6717 ± 13
42	145	2535	IC4041	13 0 40.7	27 59 47.9	S0	S0	15.93	1.90	206	0.45 ± 0.11	1.50 ± 0.24		7056 ± 11
43		2201		13 1 13.5	27 54 51.4		E	16.86	1.85	70	0.24 ± 0.12	1.62 ± 0.48		5852 ± 10
44	172	2839	IC4021	13 0 14.6	28 2 28.6	E	E	16.01	1.75	397	0.19 ± 0.07	2.31 ± 0.18		5689 ± 13
45	207	2912		13 0 8.9	28 10 13.2	E	E	16.07	1.80	226	0.32 ± 0.11	2.17 ± 0.22		6756 ± 12
47	130	3352	NGC4872	12 59 33.9	27 56 47.3	E/S0	E	14.74	1.93	290	0.28 ± 0.08	1.80 ± 0.19		7205 ± 14

TABLE 1. (a) (continued)

Spectrum	D	GMP	other	RA (2000)	Dec (2000)	Morph. D	Morph. C	b	b-r	Signal	CN/H8	Hδ (Å)	A?	$V_\odot$ (km s^{-1})
49	142	2048		13 1 27.0	27 59 57.6	E	E:	17.06	1.94	87	0.55 ± 0.25	2.00 ± 0.46		7558 ± 13
50	53	3697		12 59 10.2	27 37 11.6	E	E	16.59	1.87	72	0.03 ± 0.16	1.65 ± 0.49		5691 ± 12
51	84	2956		13 0 5.3	27 48 26.8	S0	S0	16.20	1.98	258	0.27 ± 0.11	2.39 ± 0.22		6548 ± 11
54	104	3296	NGC4875	12 59 37.8	27 54 26.5	S0	E	15.88	1.96	163	0.54 ± 0.14	2.37 ± 0.29		8056 ± 13
55	121	2798		13 0 17.6	27 57 19.5	E	E	14.85	2.62	248	0.49 ± 0.06	1.81 ± 0.22		6811 ± 14
56	156	3471		12 59 26.4	27 59 54.3	E/S0	E/S0	16.45	1.84	164	0.50 ± 0.12	2.75 ± 0.29		6665 ± 9
57	91	3997	IC3946	12 58 48.5	27 48 37.3	S0	S0	15.28	1.95	572	0.46 ± 0.07	2.19 ± 0.18		5916 ± 16
58	159	3664	NGC4864	12 59 13.0	27 58 37.2	E	E	14.70	2.30	291	0.48 ± 0.09	1.86 ± 0.18		6806 ± 13
59	152	3170	IC3998	12 59 46.6	27 58 25.9	SB0	S0	15.70	1.90	226	0.22 ± 0.07	1.95 ± 0.24		9401 ± 11
60	179	3561	NGC4865	12 59 19.7	28 5 3.8	S0	S0	14.54	1.83	501	0.38 ± 0.08	2.07 ± 0.18		4609 ± 17
61	192	2584		13 0 35.5	28 8 46.4	S0	S0	16.14	1.79	50	0.17 ± 0.11	2.50 ± 0.56		5441 ± 11
62	118	2541	NGC4906	13 0 39.5	27 55 26.5	E	E	15.44	1.98	267	0.54 ± 0.10	2.23 ± 0.20		7494 ± 14
64	116	2510		13 0 42.7	27 57 47.5	SB0	E/S0	16.13	1.90	28	0.49 ± 0.13	1.91 ± 0.32		8366 ± 9
65	216	2989		13 0 2.8	28 14 25.0	Sa	S0	17.05	1.88	109	−0.70 ± 0.13	2.30 ± 0.33	√	7684 ± 7
66	124	3201	NGC4876	12 59 44.3	27 54 44.6	E	E/S0	15.51	1.91	221	0.10 ± 0.08	1.77 ± 0.23		6629 ± 11
68	103	3400	IC3973	12 59 30.6	27 53 3.2	S0/a	E/S0	15.32	1.88	662	0.33 ± 0.08	1.96 ± 0.18		4692 ± 16
69	90	3943		12 58 52.9	27 48 48.2	S0	S0	16.93	1.88	89	0.24 ± 0.11	2.00 ± 0.41		5496 ± 11
70	177	3433		12 59 28.6	28 2 26.1	S0	S0	16.56	1.79	77	0.02 ± 0.16	2.50 ± 0.47		5569 ± 11
73	160	3761	IC3955	12 59 5.9	27 59 48.2	SB0	S0	15.57	1.88	245	0.42 ± 0.09	1.88 ± 0.21		7650 ± 12
74	72	3958	IC3947	12 58 52.0	27 47 6.2	E	E/S0	15.94	1.91	146	0.61 ± 0.12	2.63 ± 0.30		5702 ± 12
76	108	3782		12 59 4.5	27 54 39.4	S0	S0	16.55	1.85	190	0.31 ± 0.07	2.20 ± 0.27		6396 ± 11
77	173	2861		13 0 12.7	28 4 31.6	S0	S0	16.26	1.85	321	0.47 ± 0.10	2.02 ± 0.18		7493 ± 10
78	98	2347		13 0 59.1	27 53 59.6	S0/a	S0	15.85	1.91	180	0.25 ± 0.07	2.70 ± 0.27		6828 ± 10
79	146	2551		13 0 38.7	28 0 51.7	SB0/a	S0	16.85	2.99	76	−0.47 ± 0.14	3.25 ± 0.48	:	7537 ± 9
81		2421		13 0 50.9	27 44 34.5		S0	17.98	1.90	35	−0.86 ± 0.19	1.50 ± 0.77		8126 ± 14
82	133	3639	NGC4867	12 59 15.0	27 58 14.9	E	S0	15.44	1.83	494	0.35 ± 0.07	2.26 ± 0.18		4793 ± 16
83	117	2457		13 0 47.2	27 55 19.5	S0/a	S0	16.56	1.88	134	−0.14 ± 0.14	2.79 ± 0.31		8571 ± 9
85	180	3656		12 59 13.7	28 4 34.9	S0	E	15.53	1.77	143	0.37 ± 0.10	1.80 ± 0.30		7790 ± 13
86	150	2940	IC4011	13 0 6.2	28 0 14.7	E	E:	16.08	1.82	199	0.30 ± 0.11	2.11 ± 0.25		7245 ± 13
88	79	2157	NGC4919	13 1 17.5	27 48 33.0	S0	S0	15.06	1.92	118	0.31 ± 0.11	1.00 ± 0.32		7317 ± 14
91		3481		12 59 25.6	28 11 12.9		E	17.69	1.68	99	0.51 ± 0.18	2.00 ± 0.38		7718 ± 11
93	147	2651		13 0 28.2	27 58 20.4	S0	S0	16.19	1.85	188	−0.29 ± 0.11	2.89 ± 0.25		7679 ± 10
94	64	2866		13 0 12.4	27 46 54.0	E	E	16.90	1.79	118	−0.21 ± 0.12	2.70 ± 0.32		6992 ± 11
95	151	2975	NGC4886	13 0 4.2	27 59 14.8	E	E	14.83	1.76	505	0.23 ± 0.09	2.83 ± 0.18		6359 ± 13
96	71	3882		12 58 57.5	27 47 7.5	S0	S0	16.97	1.85	72	0.34 ± 0.16	2.94 ± 0.48		6894 ± 12
97	175	3073	NGC4883	12 59 55.9	28 2 4.9	S0	E	15.43	1.89	217	0.47 ± 0.11	2.07 ± 0.24		8071 ± 13

TABLE 1. (b) Coma galaxies in the SW field.

Spectrum	D	GMP	other	RA (2000)	Dec	Morph. D	Morph. C	b	b-r	Signal	CN/H8	Hδ (Å)	A?	$V_\odot$ (km s^{-1})
3		4083		12 58 40.7	27 49 37.8		S0	17.82	1.91	9	−2.13 ± 0.72			6254 ± 54
4		4578		12 57 56.3	27 22 56.0		E/S0	18.04	1.80	15	0.58 ± 0.48			5186 ± 29
5		4330		12 58 20.4	27 25 46.1		S0:	17.96	1.67	26	−0.96 ± 0.18	1.50 ± 1.19	√	7601 ± 71
8		5284		12 56 42.2	27 32 53.6		S0	17.98	1.75	24	0.21 ± 0.37	2.50 ± 1.23		7545 ± 37
9	24	5051		12 57 9.4	27 27 58.8	E	E/S0	15.46	2.07	127	0.77 ± 0.09	2.39 ± 0.31		7444 ± 15
11	21	4522		12 58 1.5	27 29 21.6	Sa	S0	15.83	1.84	61	−0.77 ± 0.33	1.80 ± 0.52	√	7606 ± 12
14		5296		12 56 40.8	27 26 51.7		S0	18.90	1.83	15	0.15 ± 0.50	2.70 ± 1.85		7310 ± 21
16		4519		12 58 1.4	27 51 12.6		S0	17.61	1.81	12	−0.87 ± 0.82			5638 ± 30
17	89	3896	IC3949	12 58 56.3	27 50 1.6	S	S0	15.13	1.75	110	−0.29 ± 0.27	4.04 ± 0.31	√	7378 ± 21
18		5100		12 57 4.1	27 43 48.4		S0:	17.15	1.71	23	−0.79 ± 0.32	3.00 ± 0.73	√	8890 ± 31
19	23	4792	NGC4842	12 57 36.0	27 29 5.3	S0	S0	16.30	1.91	141	0.14 ± 0.12	1.87 ± 0.31		7234 ± 14
20		4972		12 57 18.1	27 44 50.4		S0:	18.07	1.79	7				6834 ± 90
21	14	4692		12 57 45.6	27 25 45.6	S0	S0:	17.37	1.74	32	−0.83 ± 0.39	3.60 ± 0.86	√	8318 ± 17
22		4479		12 58 5.9	27 25 7.7		S0	17.51	1.83	27	−0.15 ± 0.22	1.31 ± 1.28		5749 ± 16
24	73	4341		12 58 19.0	27 45 42.9	E	S0	17.33	1.84	63	−0.52 ± 0.23	3.23 ± 0.52	√	5434 ± 10
25	20	4206		12 58 31.9	27 27 22.8	S0	S0	16.41	1.90	125	0.67 ± 0.12	3.00 ± 0.33		7035 ± 11
26	32	4943		12 57 22.7	27 29 34.9	S0	S0	15.88	1.83	94	0.37 ± 0.08	2.71 ± 0.40		8241 ± 12
27	33	4907		12 57 25.9	27 32 45.1	S0	S0	15.93	2.20	76	0.70 ± 0.14	2.05 ± 0.46		5475 ± 13
28	92	4499		12 58 3.4	27 48 53.6	E/S0	S0	16.10	1.82	125	0.60 ± 0.10	1.84 ± 0.32		7095 ± 14
31	15	4918	Mrk55	12 57 25.2	27 24 16.4	S0	S0	16.03	1.47	91	−0.28 ± 0.16	4.54 ± 0.37[a]	√	4811 ± 55
32	35	5364	NGC4824	12 56 34.0	27 32 20.2	E	S0	15.96	2.01	138	0.60 ± 0.12	2.34 ± 0.32		7116 ± 14
34	76	4933		12 57 23.3	27 45 58.5	SBa	S0	16.35	1.90	48	−0.83 ± 0.25	2.53 ± 0.61		9107 ± 13
35	46	4829	NGC4840	12 57 32.7	27 36 37.0	E/S0	E:	14.86	1.98	350	0.71 ± 0.09	1.50 ± 0.18		6055 ± 20
37		4215		12 58 31.5	27 23 41.6		S0	18.82	1.66	10	−2.58 ± 0.81	5.86 ± 1.93		7554 ± 35
38		4294		12 58 25.2	27 11 59.8		E/S0	17.64	1.72	20	−1.45 ± 0.39	2.29 ± 1.32	:	8045 ± 42
39	93	4664		12 57 47.3	27 49 58.3	S0	S0	16.26	2.06	77	0.81 ± 0.13	2.51 ± 0.45		6118 ± 11
40	112	4945		12 57 21.6	27 52 49.5	E	S0	16.64	1.78	97	−0.90 ± 0.15	4.40 ± 0.33	√	7428 ± 8
42	43	4156	NGC4853	12 58 35.2	27 35 47.1	S0p	E?	14.38	1.66	379	−0.81 ± 0.10	3.84 ± 0.18[b]	√	7660 ± 14
43		3588		12 59 18.3	27 30 48.4		S0	17.76	1.72	17	−0.14 ± 0.39	2.83 ± 1.52		6076 ± 20
44	71	3882		12 58 57.5	27 47 7.5	S0	S0	16.97	1.85	50	0.14 ± 0.27	1.70 ± 0.60		6916 ± 11

[a] Uncorrected value is 1.49. [b] Uncorrected value is 3.27.

TABLE 1. (b) (continued)

Spectrum	D	GMP	other	RA (2000)	Dec	Morph. D	Morph. C	b	b-r	Signal	CN/H8	Hδ (Å)	A?	$V_\odot$ (km s^{-1})
50		4630		12 57 50.6	27 29 27.2		E	18.97	1.92	25	0.39 ± 0.46	3.00 ± 1.29		7335 ± 17
55	42	3879		12 58 57.8	27 35 40.6	S0	S0	16.31	1.86	79	0.30 ± 0.16	2.76 ± 0.49		5967 ± 13
57		4956		12 57 21.5	27 28 28.8		E	18.52	1.73	23	2.05 ± 0.41	2.00 ± 1.36		6902 ± 17
60	45	4579		12 57 56.1	27 34 52.3	Sa	S0:	16.72	1.80	48	−0.89 ± 0.09	5.20 ± 0.54[c]	✓	4915 ± 53
61	72	3958	IC3947	12 58 52.0	27 47 6.2	E	E/S0	15.94	1.91	167	0.55 ± 0.09	2.22 ± 0.29		5663 ± 12
63		5320		12 56 38.3	27 34 15.4		S0	18.80	1.81	17	−0.76 ± 0.44	0.94 ± 1.36		7625 ± 25
64	44	4255		12 58 28.2	27 33 34.0	S0	S0	16.57	1.77	77	−1.27 ± 0.17	3.78 ± 0.46[d]	✓	7534 ± 18
65		4502		12 58 3.4	27 40 56.6		S0:	18.02	1.95	41	0.56 ± 0.17	2.80 ± 0.85		7209 ± 12
68		5012		12 57 13.9	27 15 13.4		S0	18.43	1.88	14	1.27 ± 0.50	1.92 ± 1.73		5174 ± 26
69	16	5038		12 57 10.6	27 24 17.6	Sa	S0	16.14	1.82	96	−0.26 ± 0.14	3.00 ± 0.37[e]	✓	6205 ± 15
70	94	4974		12 57 17.8	27 48 39.2	S0	S0	16.49	1.62	50	−1.20 ± 0.17	2.50 ± 0.55	✓	7084 ± 11
72	22	4597		12 57 54.1	27 29 26.4	SBb	S0	16.37	1.91	29	−0.86 ± 0.13	3.41 ± 0.92		4915 ± 25
73	60	5362		12 56 34.0	27 41 14.4	E	S0:	17.77	1.89	31	0.01 ± 0.29	0.74 ± 1.05		6843 ± 16
74		5136		12 57 1.5	27 22 19.3		S0	16.62	2.00	70	0.30 ± 0.17	3.12 ± 0.50		7012 ± 10
75		4420		12 58 11.3	27 56 23.9		E/S0	17.60	1.86	45	−0.32 ± 0.16	2.61 ± 0.60		8509 ± 15
76	34	5102		12 57 4.2	27 31 33.2	S0	S0	17.50	1.92	34	−0.91 ± 0.14	2.69 ± 1.00	:	8328 ± 14
77	91	3997	IC3946	12 58 48.5	27 48 37.3	S0	S0	15.28	1.95	185	0.35 ± 0.10	2.03 ± 0.28		5983 ± 14
78	29	4447		12 58 9.7	27 32 57.7	E	S0:	17.81	1.98	22	0.15 ± 0.43	5.97 ± 1.30		6958 ± 18
79		4469		12 58 6.7	27 34 37.1		S0:	17.69	1.88	19	−1.24 ± 0.50	2.96 ± 1.57		7452 ± 22
80		4535		12 58 0.6	27 27 14.4		E/S0	17.90	1.95	44	−0.28 ± 0.29	2.01 ± 0.69		7653 ± 13
82		5546		12 56 14.5	27 30 22.6		S0	17.42	1.93	38	−0.55 ± 0.30	1.88 ± 0.68		7429 ± 23
83	28	4117		12 58 38.2	27 32 38.8	E/S0	S0	16.67	1.99	101	0.39 ± 0.13	3.14 ± 0.37		5962 ± 11
84	74	4656		12 57 47.7	27 46 10.0	E	S0	17.62	1.82	41	−0.27 ± 0.21	1.76 ± 0.71		5764 ± 14
85	77	5096		12 57 4.4	27 46 22.7	S0/a	S0	16.89	1.78	41	−0.80 ± 0.15	2.50 ± 0.69	✓	7544 ± 28
86	69	3730	IC3959	12 59 8.0	27 47 2.7	E	E	15.27	1.94	199	0.97 ± 0.09	1.72 ± 0.26		7042 ± 20
90		4714		12 57 43.1	27 34 39.3		E/S0:	17.54	1.75	60	−0.45 ± 0.17	3.22 ± 0.55		7226 ± 18
91	75	4679		12 57 46.0	27 45 25.4	S0	S0	16.13	1.91	69	0.81 ± 0.13	1.39 ± 0.50		6123 ± 12
93	53	3697		12 59 10.2	27 37 11.6	E	E	16.59	1.87	124	0.88 ± 0.11	2.85 ± 0.32		5730 ± 13
96	30	4794	NGC4842	12 57 35.6	27 29 36.1	S0	E	15.26	2.02	167	0.44 ± 0.11	2.39 ± 0.29		7343 ± 17
97		4314		12 58 21.8	27 53 32.2		S0	17.66	1.88	24	−1.56 ± 0.44	3.23 ± 1.16		7252 ± 27

[c] Uncorrected value is 1.58. [d] Uncorrected value is 3.35. [e] Uncorrected value is 2.13.

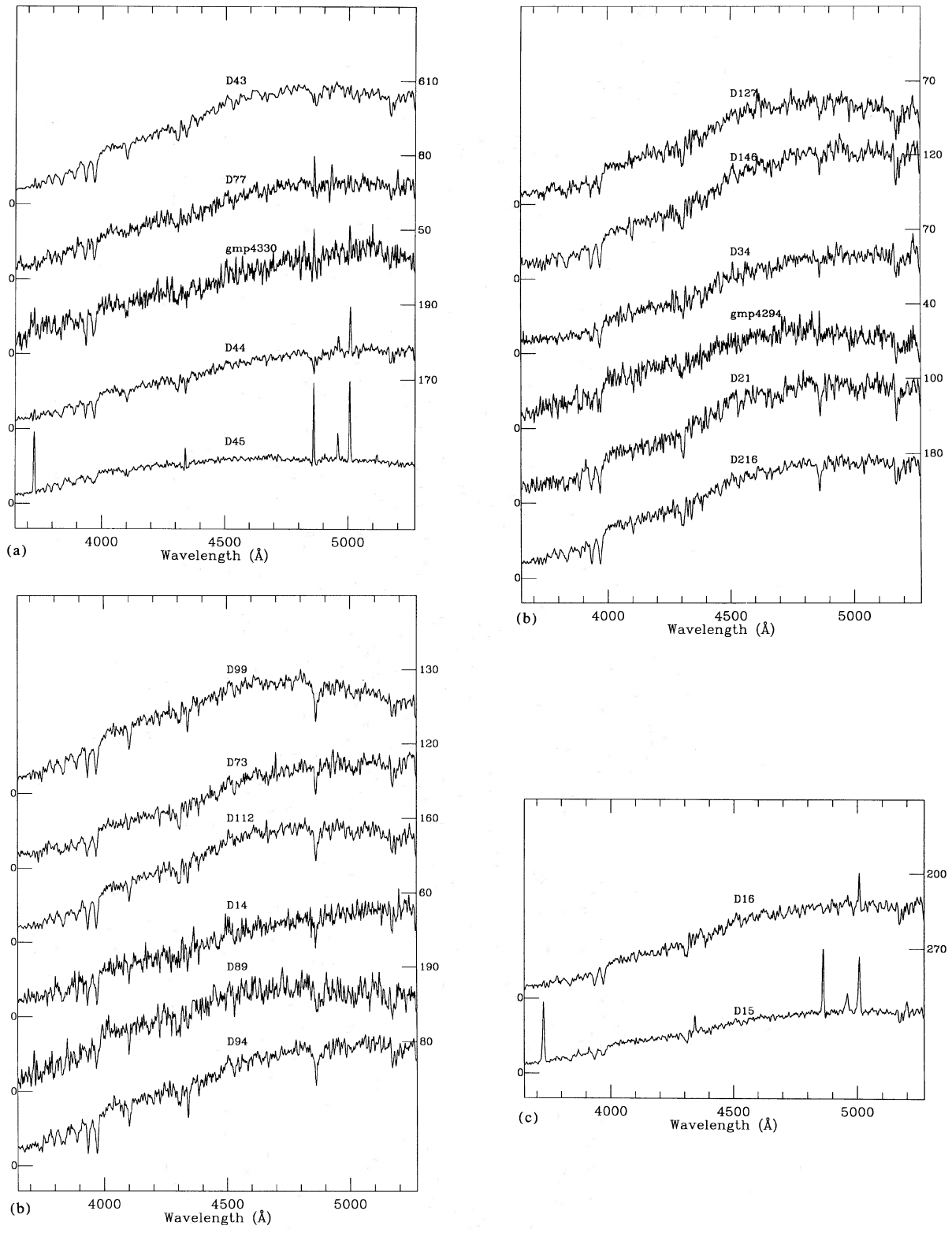

Fig. 2. (a) Spectra of Coma galaxies with enhanced Balmer absorption lines and emission lines. (b) Spectra of Coma galaxies with enhanced Balmer absorption but no detectable emission. (c) Spectra of Coma galaxies with emission spectrum dominated by an AGN. (d) Several representative spectra of Coma galaxies with normal spectra for early-type galaxies.

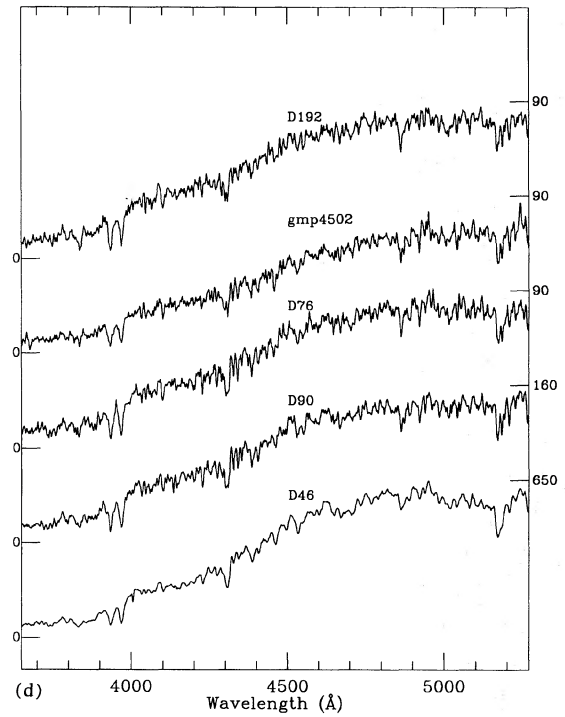

FIG. 2. (continued)

2), to make a valid comparison between the two fields, we will restrict our discussion to a fixed magnitude range in which a large number of galaxies were observed in both fields. Inspection of Fig. 1 suggests that for $B < 17.2$ the luminosity distributions will be very similar; additionally the S/N ratio will be more uniform in the samples. Fainter than this limit, 23 galaxies were observed in the SW field, but only 6 in the central field. Applying this additional magnitude cut leaves 68 galaxies in the central field and 28 in the SW field. In Sec. *3.3* we briefly return to some interesting aspects of the 23 faint galaxy spectra in the SW field. Otherwise, in future discussions we refer only to the $B < 17.2$ samples.

To quantify the amount and nature of the emission in our spectra, we measured equivalent widths and line ratios for the prominent star-formation indicators. The most reliably quantifiable emission features are [O II]λ3727 and [O III]$\lambda\lambda$5007,4959 since often the Balmer emission lines are superposed on enhanced Balmer absorption. These values are presented in Table 2. In order to explore quantitatively the enhanced Balmer absorption, we constructed two indices from high order lines: (1) the equivalent width of Hδ, and (2) a slope index which essentially measures the depth of the H8 line (λ3889) relative to the usually dominant CN 3883 bandhead (we refer to this index as CN/H8). Both indices are listed in Table 1. We begin our analysis with the Hδ equivalent width, since the use of that feature for the detection of young stars in integrated spectra of galaxies should be familiar to most readers. However, experiments with synthetic spectra show that, if sufficient S/N is available shortward of 4000 Å, the second

TABLE 2. Emission line data.

		D15	D16	D44	D45
[OII]λ3727	EW (Å)	54.7	1.4	2.6	34.0
	Flux (counts)	1506.8	40.3	64.4	682.0
[NeIII]λ3869	EW (Å)	1.4			
	Flux (counts)	104.2			
Hδ	EW (Å)	1.7			3.0
	Flux (counts)	439.2			
Hγ	EW (Å)	3.4			4.9
HeIIλ4686	EW (Å)		0.8		
	FWHM (km s^{-1})		142		
Hβ	EW (Å)	10.2	0.5	1.5	15.0
	Flux (counts)	439.2	< 21	59.3	5.2
	FWHM (km s^{-1})	204			*
[OIII]λ4959	EW (Å)	3.3	1.0	1.3	3.8
	Flux (counts)	247.7			
	FWHM (km s^{-1})		216	145	143
[OIII]λ5007	EW (Å)	9.0	3.0	4.4	11.9
	Flux (counts)	490.2	140.9	187.5	291.0
	FWHM (km s^{-1})	416	245	203	106

* Width is unresolved.

index is more reliable at detecting the presence of hot stars, since it is less affected by Balmer emission fill-in. We therefore present a more complete discussion below using the CN/H8 index.

Figure 3 shows histograms of the Hδ equivalent widths (hereafter referred to simply as Hδ) for the galaxies in the central and SW fields with $B < 17.2$. These values were measured automatically by defining a central bandpass

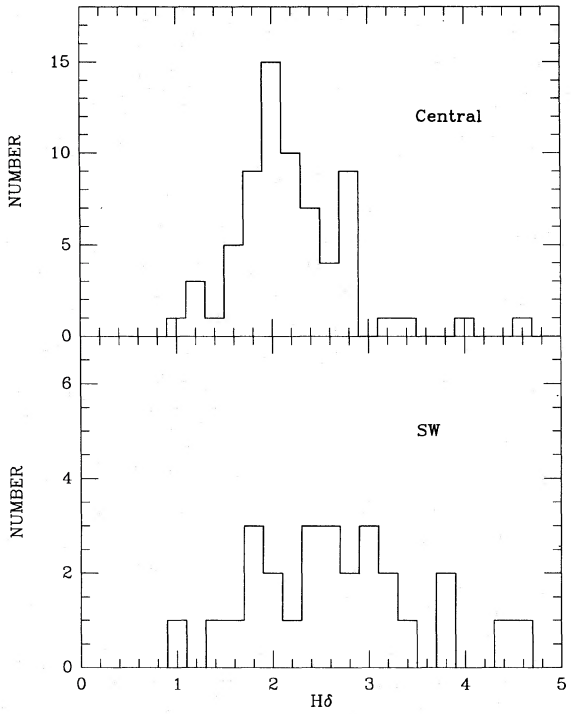

FIG. 3. Histograms of the Hδ equivalent width indices for (a) galaxies in the central field and (b) galaxies in the SW field brighter than $B = 17.2$.

between 4092 and 4115 Å with sidebands from 4088 to 4092 Å and 4115 to 4120 Å. The errors were determined by creating 100 artificial spectra with Hδ lines containing random noise equivalent to that in the real spectrum, and measuring the dispersion about the input value. In a few cases, where instrumental artifacts were present, the Hδ equivalent width was measured using an interactive feature in the IRAF "splot" task. Five galaxies showed evidence of substantial emission fill-in of Hδ lines. For these galaxies a suitable emission-free spectrum (usually the composite of several spectra) was first used to remove the underlying absorption spectrum, in order that the Hβ emission flux could be measured (this is the lowest order Balmer line in our spectrum and hence the one where emission most dominates over absorption). A Case B Balmer decrement from Osterbrock (1974) was then used to calculate the emission flux in Hδ, from which a correction to the Hδ absorption equivalent width measurement could be obtained. These corrected values are listed for the five galaxies in Table 1, while the uncorrected values are listed in footnotes.

The great majority of the galaxies in the central field have Hδ indices clustered around 2 Å, whereas those in the SW field show a significant spread to larger equivalent widths. A Kolmogorov–Smirnov two-sample test rejects the hypothesis that the two Hδ distributions are drawn from the same parent population at the 1.3% confidence level. In short, a substantially higher fraction of early-type galaxies in the SW field show enhanced Balmer absorption lines than do their counterparts in the central field of the cluster.

To lend further support to this result we now turn to the CN/H8 slope index. Since H8 is two Balmer lines farther down the decrement, it is about four times less affected by emission than Hδ. In fact, no correction for emission fill-in was made to the CN/H8 indices of the five galaxies for which corrections to the Hδ equivalent widths were made. In detail, the CN/H8 index is a least-squares fit to the slope of the spectrum between 3858 and 3893 Å, normalized to a unit continuum at the center of the band, and multiplied by 100 for convenience. This wavelength region encompasses all of the CN3883 feature, and most of the H8 line (all of the blueward half and part of the redward half). For normal early-type galaxy spectra, which are dominated by cool stars, CN completely dominates over H8, so that the spectrum has the characteristic downward slope to shorter wavelength of the CN band. But when early F and A stars are added, H8 is greatly strengthened and CN diluted, so a strong shift in slope occurs, giving the index its large dynamic range. This change in spectral slope is illustrated in Fig. 4, which shows a normal E/S0 spectrum in that wavelength range, as well as a spectrum showing strong Balmer absorption. It may seem that the index would be sensitive to errors in the exact placement of the wavelength interval over which the slope is measured. However, shifting the wavelength interval by 1 and 2 pixels (i.e., 1 and 2 Å at our dispersion) in either direction, causes the index to change by only ±0.03 for 1 Å shifts and ±0.07 for 2 Å shifts. Hence it is quite stable to small errors in defining the wavelength interval, at least at our

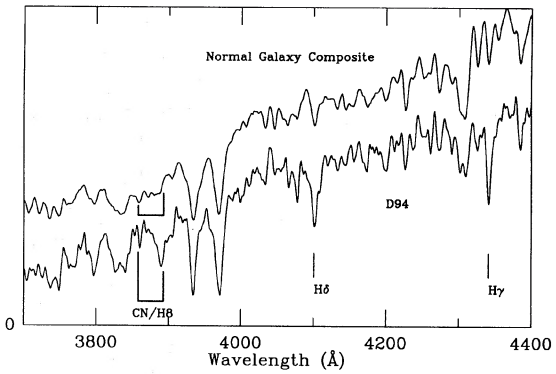

FIG. 4. Comparison of (a) normal and (b) enhanced Balmer absorption spectra in the CN/H8 wavelength region.

spectral resolution. In Fig. 5 we have plotted Hδ versus the CN/H8 index for the galaxies in both the central and SW fields and there is clearly a good correlation between the two indices. The CN/H8 index was measured on all of the spectra, and is listed in Table 1.

To further demonstrate the excess of galaxies with unusually strong Balmer absorption in the SW region of Coma, histograms of the CN/H8 slope indices for both the SW and the central fields are plotted in Fig. 6. Once again it is apparent that the galaxies in the SW field contain a high fraction of spectra which have enhanced Balmer absorption. The two-sample Kolmogorov–Smirnov test rejects the hypothesis that both SW and central field samples are drawn from the same parent distribution at the 2.8% confidence level. Although formally not as significant as that obtained using Hδ, no corrections for emission fill-in were required in this case.

Henceforth, we consider all spectra with CN/H8 indices less than −0.5 to be "abnormal." Also classified as abnormal are two AGN spectra in the SW region (which are further discussed in Sec. *3.2.1*); no AGN spectra were

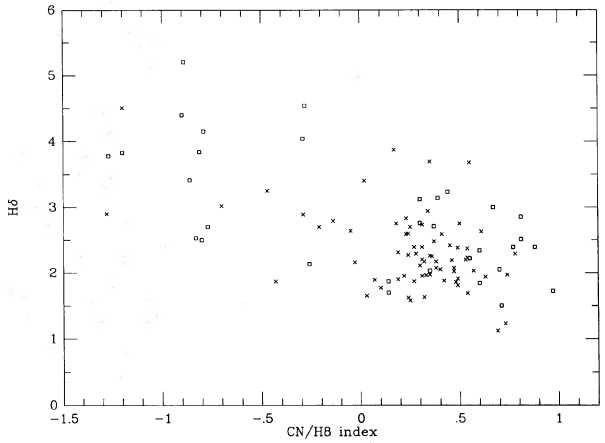

FIG. 5. The Hδ index is plotted as a function of the CN/H8 index to demonstrate the correlation between the two indices. The crosses refer to galaxies in the central field and the squares refer to galaxies in the SW field.

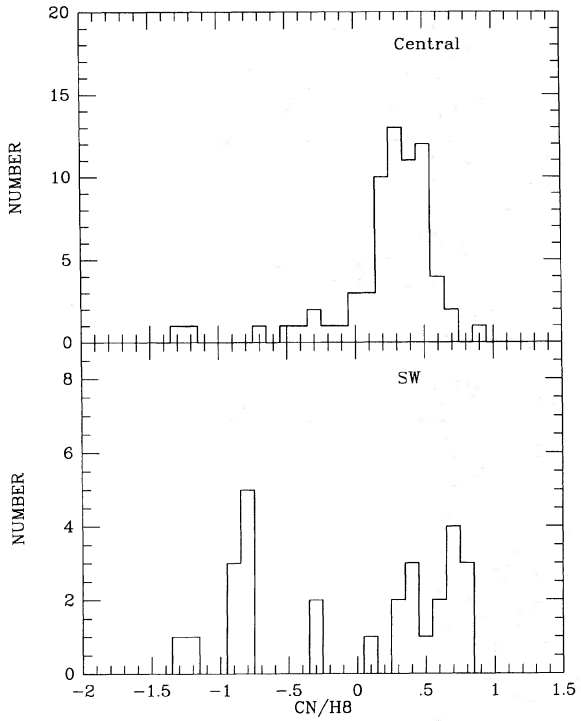

FIG. 6. Histograms of the CN/H8 indices for (a) all galaxies with $B \leqslant 17.2$ in the SW field and (b) all galaxies with $B \leqslant 17.2$ in the central field.

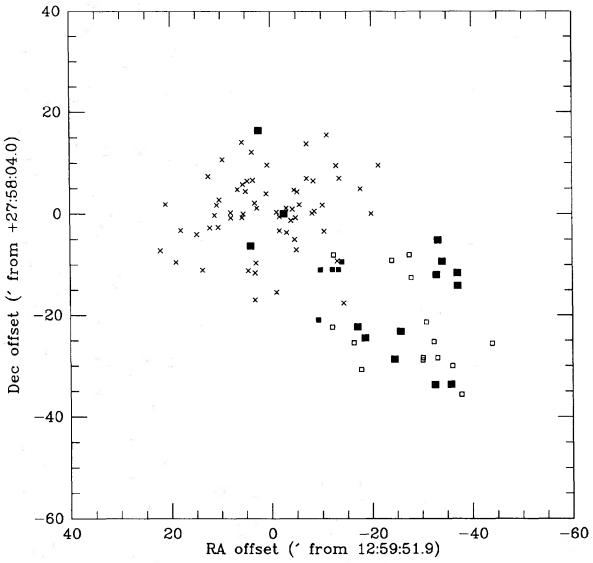

FIG. 7. Positions of Coma galaxies with $B \leqslant 17.2$ observed with Hydra, referred to the cluster center. SW field galaxies are plotted as open squares, and central field galaxies are plotted as crosses. Filled symbols are abnormal-spectrum galaxies.

found among the galaxies observed in the central field. According to these criteria, 11 out of the 28 galaxies (39%) in the SW region with $B < 17.2$ are abnormal, as opposed to only 3 out of 68 (4%) in the central field. Figure 7 shows the sky positions of all abnormal-spectrum $B < 17.2$ galaxies together with their normal counterparts. The spatial segregation is clearly seen.[2]

3.2 Comparison with Spectra of Other Stellar Systems

3.2.1 Comparison with normal spirals

Given the large number of Coma galaxies with unusual spectra, it is important to look for spectral analogs in other galaxies which might clarify the physical phenomena we are observing. It is also clear from Fig. 8 that, despite the strict color selection by which the majority of the galaxies were selected, the abnormal-spectrum galaxies in the SW field are slightly bluer than their normal counterparts. This raises the question of spiral contamination given that most of the abnormals are in the SW field and there is a change in the morphological fractions with radius (Caldwell & Oemler 1981). In particular, several of the abnormal-spectrum galaxies were classified as S0/a or Sa by Dressler, and it is conceivable that the distance of Coma has caused others to be erroneously classified as S0's. We will establish in this section that the abnormal spectra are *not* typical of normal spirals and that, morphologically, there is no question that the large majority of the SW sample are early-type E or S0 galaxies. To address the question of morphological errors, we obtained *R*-band CCD images of many of the abnormal galaxies with the 1.2-m telescope on Mt. Hopkins. These are displayed in Fig. 9 (Plate 14) and described in more detail in Appendix A. We simply comment here that the frames tend to justify the classifications presented in Table 1, but still leave room for misclassification based on the poor resolution caused by Coma's distance and the red passband used.

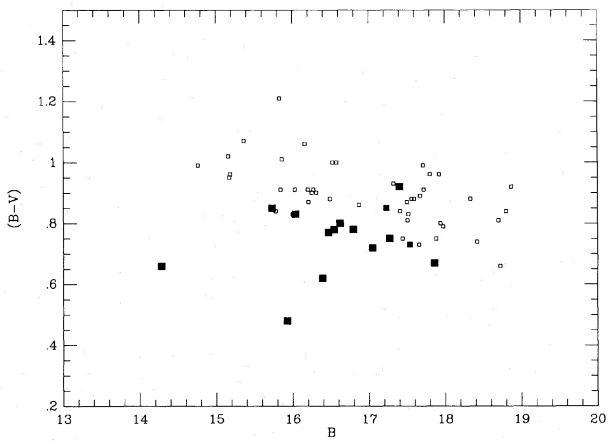

FIG. 8. $(B-V)$ vs B for Coma galaxies in the SW field only, with open squares denoting the normal-spectrum galaxies, large filled squares representing the unambiguous abnormal-spectrum galaxies, and smaller filled squares representing uncertain cases.

[2]Furthermore, it is interesting that one of the three abnormal-spectrum galaxies in the central field (D99) has a velocity of 9900 km s^{-1}, nearly 3σ higher than the mean velocity of the cluster. Thus this galaxy may in fact be falling in on the near side of the cluster, and not really be associated with the cluster center.

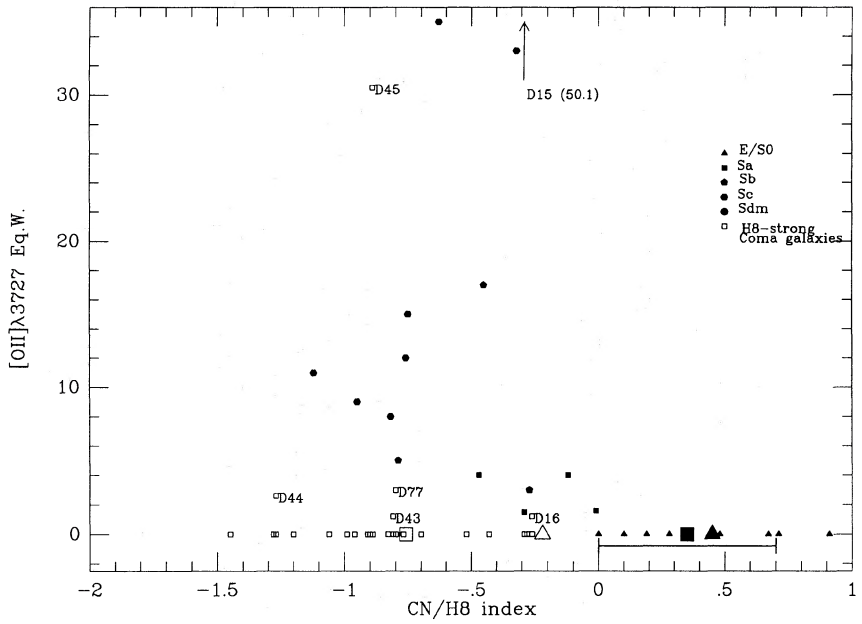

FIG. 10. Equivalent width of [O II]λ3727 vs CN/H8 index for Coma abnormal galaxies (open squares) and Kennicutt galaxies (various filled symbols for different morphological types). The larger symbols refer to the composite spectra described in Sec. 3.2.

We can also address the issue of possible misclassifications through a comparison of our spectra with those of a representative sample of normal galaxies such as that obtained by Kennicutt (1992a). Kennicutt's sample covers a complete range of morphological types, so we can test whether our spectra resemble those of any type of normal galaxy. Each Kennicutt spectrum covers the disk and bulge of the galaxies, whereas each Coma spectrum with the 2″ aperture covers only the central 0.7 kpc (for a distance of 69 Mpc, or $H_0=100$ km s^{-1} Mpc^{-1}), where the bulge of a disk galaxy would dominate. Thus, this comparison would tend to make the spectrum of a Coma S0 with nuclear star formation (abnormal) appear similar to that of a (normal) spiral, since Kennicutt's spectra of the latter include the star-forming disk. Therefore, real spectral differences seen between the Coma galaxies and the Kennicutt sample are highly significant.

Specifically, we have compared the strength of the Balmer absorption (measured by the CN/H8 index) with the strength of emission (measured from the equivalent width of [O II]λ3727). In principle, these should be correlated since both [O II]λ3727 emission and enhanced Balmer absorption are byproducts of star formation. The [O II] and CN/H8 data for the Coma data and the Kennicutt data are plotted in Fig. 10. For clarity, the location of the normal Coma spectra has been indicated by a bar, where the length of the bar includes 95% of the sample. [O II] equivalent widths for the Kennicutt galaxies have been taken from his Table 1 (Kennicutt 1992b), while the CN/H8 indices were measured directly from the original spectra. We excluded galaxies in his sample classed as morphologically peculiar (e.g., as Ep, S0p, etc.). The main feature of Fig. 10 is that virtually all of the abnormal Coma galaxies lie in a region distinct from the locus of normal galaxies defined by Kennicutt's sample, because their [O II] emission is too weak for the Balmer absorption strength (as characterized by the CN/H8 index). Thus, even if some of the abnormal-spectrum galaxies have later morphological types than S0, their spectra are still unusual. This trend for the abnormal Coma galaxies to lie in a region distinct from the Kennicutt galaxies is also confirmed by a plot of CN/H8 against $B-V$) color (Fig. 11), where the Coma galaxies are found to be generally redder than the Kennicutt galaxies at a given value of CN/H8.

There are three abnormal-spectrum Coma galaxies that merit further discussion because they overlap with the Kennicutt spirals in Fig. 10:

(i) D16 has a low-luminosity Seyfert 2 emission spectrum, as evidenced by its high excitation and the presence of He II 4686 (see Appendix A for details). This is highly unusual, both because the Seyfert 2 phenomenon is present in such a low-luminosity host galaxy ($M_B\approx -18.1$) and because the emission line to galaxy continuum ratio is so low, e.g., the equivalent width of [O III]λ5007 is only 2.5 Å. In fact, the Seyfert characteristics of D16 approach those of NGC 4395 (Filippenko & Sargent 1989) and G1200-2038 (Kunth *et al.* 1987), the two most extreme "dwarf" Seyfert galaxies studied to date.

(ii) D15, although overlapping with later-type Kennicutt spirals in Fig. 10, is far too extreme in its emission-line properties for its S0 morphological classification, or even for an Sa. While the morphological classification may be subject to some error, D15 is certainly not an Sb or Sc.

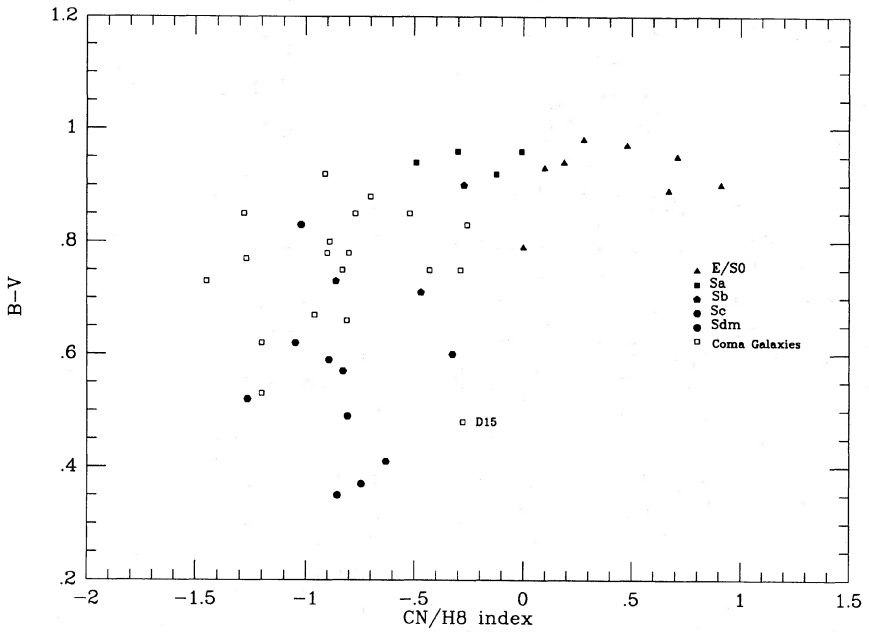

FIG. 11. $B-V$ vs CN/H8 slope index for Coma abnormal and Kennicutt galaxies.

(iii) D45, classified as Sa by Dressler (1980a), has emission lines much too strong for both its morphology and its red color. The latter effect is seen in Fig. 12, where the $B-V$ colors of the Kennicutt galaxies are plotted versus [O II] equivalent width.

In summary, none of the abnormal-spectrum Coma galaxies have characteristics similar to those of "normal" spirals, thus we are not simply witnessing a manifestation of the morphology–radius relation in clusters.

We have also compared our spectra of the galaxies classified as S, S0/a, or Sa by Dressler (1980a) as a function of location in the cluster. We find that four out of seven such galaxies in the SW region have abnormal spectra, as opposed to only one out of six in the central region. This

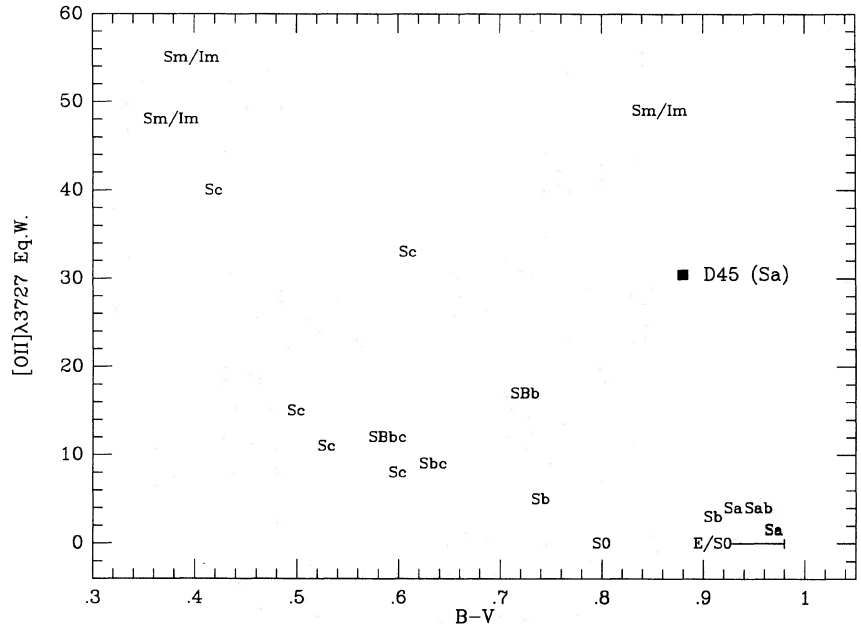

FIG. 12. [O II]λ3727 versus $B-V$ for Kennicutt galaxies and for the Coma abnormal-spectrum D45. Note that D45 is much redder for the [O II] equivalent width than the Kennicutt galaxies.

further bolsters the point that the SW field has more abnormal-spectrum galaxies than does the central region, even if some of these galaxies have morphological types which are later than S0.

3.2.2 Comparison with distant cluster galaxies

In the previous section, we showed that the abnormal galaxies that we have identified in the Coma cluster are not simply misclassified spiral galaxies and appear to require a more complex star-formation history for their explanation. The abnormal absorption-line spectra are reminiscent of the "E+A" galaxies found in $z \approx 0.3$–0.5 clusters. Dressler (1987), Gunn & Dressler (1988), and MacLaren *et al.* (1988) have defined E+A galaxies (also referred to as "post starburst") to be galaxies with intermediate colors ($B-V=0.6$–0.8) whose spectra show normal strengths of the prominent metallic features (e.g., G band, Mg b), but unusually strong Balmer absorption lines (equivalent width of $H\beta+H\gamma+H\delta \approx 7$ Å) and no emission lines. An intense short-lived episode of star formation in a galaxy with an otherwise old population can lead to such a spectrum, where the massive stars have expired leaving no stars to supply ionizing radiation, but with a plenitude of longer-lived A stars dominating the blue spectral features.

Given that our Coma galaxies were largely selected to have normal E/S0 colors, they clearly are not exact analogs to the E+A galaxies defined above. However, in their study of three clusters at $z \approx 0.3$, Couch & Sharples (1987, hereafter referred to as CS) isolated a population of photometrically *red* galaxies that also have the enhanced Hδ absorption characteristic of the E+A spectra. Figure 13 shows two composite spectra, one formed from the red Hδ-strong spectra

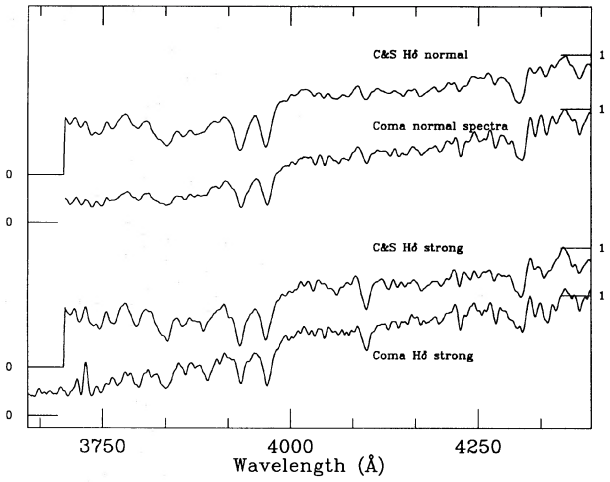

FIG. 13. Composite spectra of red, Hδ-strong CS and Coma galaxies and normal CS and Coma galaxies.

in the CS data, the other from the galaxies in the Coma sample that are within 0.15 mag of the Coma E/S0 color–magnitude sequence and have strong Hδ (D44, D77, D216, etc.). The similarity of these spectra give us confidence that we are observing essentially the same phenomenon. To further show their similarity, and the distinction from the set of standard spectra of Kennicutt (1992a), the CN/H8 indices for these two spectra are also plotted in the [O II]λ3727 vs CN/H8 diagram in Fig. 10. The CN/H8 index for the composite of red Hδ-strong CS spectra is -0.22 ± 0.13 (plotted as a large open triangle), compared

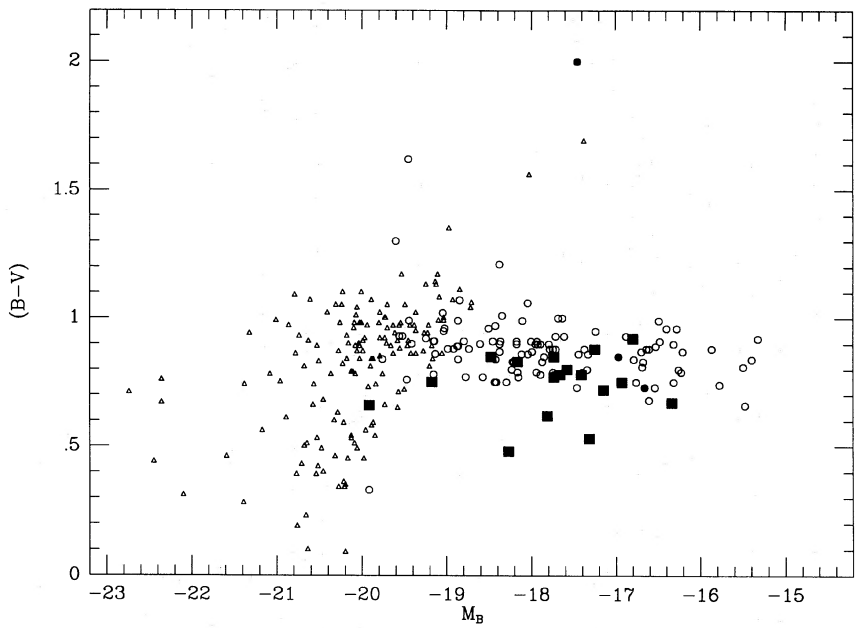

FIG. 14. $(B-V)$ vs M_B for CS galaxies (open triangles), Coma normal galaxies (open circles), and abnormal-spectrum Coma galaxies (filled squares). Smaller filled symbols represent uncertain abnormal spectra. The red magnitude selection criterion of the CS galaxies causes the diagonal faint cutoff in this B magnitude diagram. A Hubble constant of $H_0=100$ km s^{-1} Mpc^{-1} has been assumed.

with 0.45 ± 0.09 for the composite of red normal-Hδ CS spectra (filled triangle). The CN/H8 index for the composite of red Hδ-strong Coma spectra is -0.76 ± 0.16 (open square), compared with 0.35 ± 0.08 (filled square) for a composite of 70 normal Coma spectra.

A further comparison with the individual galaxies in the CS study is shown via the color–magnitude diagram of Fig. 14, in which the CS galaxies are compared to the Coma galaxies. The $(B_J - R_F)$ colors in CS were transformed to $B-V$ at $z=0$ via $(B-V) = -0.23 + 0.48(B_j - R_f)$, which was calculated by convolving the Pence (1976) and Coleman *et al.* (1980) mean spectral energy distributions (as a function of morphological type) with the filter bandpasses. There are clearly very few Coma galaxies that are as bright as the bulk of the CS galaxies. Therefore, the majority of the Coma galaxies with abnormal spectra that we observed are in a mostly unexplored region of the luminosity function of galaxies in clusters, and of distant galaxy clusters in particular. This appears to be the sole difference between the red Hδ-strong galaxies identified by CS in $z=0.3$ clusters and the red Hδ-strong galaxies in the SW region of Coma.

We have elected to include the two AGN spectra galaxies that do not also have strong Balmer absorption (D15 and D16) in the abnormal Coma group, partly because AGN's were part of the Dressler & Gunn (1983) definition of Butcher–Oemler galaxy peculiarities, but also because the Coma SW region AGN's represent a spectral class not seen in the center of the cluster. However, we note that the importance of AGN's in the distant clusters now rests entirely with the three AGN's discovered in the 3C295 cluster, as observations of other clusters have not borne out the high AGN frequency as a general phenomenon of the Butcher–Oemler effect (Lavery & Henry 1986).

3.3 Luminosity Function of Abnormal-Spectrum Galaxies

We now investigate whether the abnormal-spectrum galaxies in Coma are concentrated at a particular luminosity or distributed over a wide luminosity range. Figure 8 shows the CM diagram for *only the SW galaxies*, distinguishing again between normal and abnormal spectra. Although the samples are small, the abnormal spectra appear evenly distributed in luminosity, corresponding to $B=14$ to 17.5. Below $B=17.5$, the S/N ratio of the spectra deteriorates rapidly, so that the detection of abnormal-spectrum galaxies rapidly becomes incomplete. We did isolate three clear-cut cases of abnormal-spectrum galaxies with $B > 17.5$ (discussed individually in Appendix A), but the lack of completeness at such luminosities prevents any conclusive statement about the frequency of abnormal spectra.

Careful examination of the spectra of galaxies fainter than 17.5 did, however, reveal that some exhibit an unusually weak H and K break. Dividing the sample on this basis, with six weak-break galaxies and eleven strong-break galaxies (excluding the three clearly abnormal-spectrum galaxies), we found the weak-break galaxies have a mean

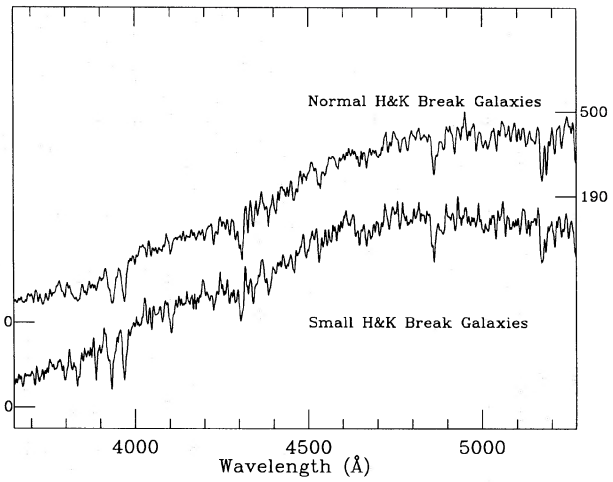

FIG. 15. Composite spectra of (a) weak-break amplitude low-luminosity Coma galaxies and (b) normal-break amplitude low-luminosity Coma galaxies.

$b-r = 1.78 \pm 0.04$, and a CN/H8 slope index of -0.82 ± 0.31, while the strong-break galaxies have a mean $b-r = 1.89 \pm 0.02$, and a CN/H8 slope of 0.06 ± 0.16. Composite weak-break and strong-break spectra have been created by coadding the individual spectra in the two groups and are plotted in Fig. 15. The strengths of the H8 and Hδ lines are particularly enhanced in the weak-break spectrum, even though the G band and Mg lines are similar. We further note that the CN/H8 index in the weak-break spectrum is similar to that in the brighter abnormal-spectrum galaxies. It is plausible, therefore, that these fainter galaxies are similar to our main sample of brighter abnormal galaxies, i.e., displaying evidence of recent star formation. If correct, the fraction of abnormal galaxies at $B \geqslant 17.5$ would increase from 3/20 to 9/20, i.e., consistent with the fraction (11/28) at brighter magnitudes ($B < 17.2$) in Sec. *3.1*. Additionally, two of the three galaxies between 17.2 and 17.5 show evidence of recent star formation; the spectrum of the third is too poor to be of much use. Higher S/N ratio spectra are required to further clarify the precise nature of these low-luminosity galaxies, but evidently the abnormal-spectrum galaxies are not confined to a narrow range in luminosity.

3.4 Spatial Distribution of the Abnormal-Spectrum Galaxies

Because our spectroscopic observations outside the central region of Coma were limited (by cloudy weather) to only the SW field, we cannot directly answer the question as to whether the abnormal-spectrum galaxies represent a localized anomaly in the galaxy population or rather are part of a general radial gradient in the stellar populations of early-type galaxies in the Coma cluster. Such knowledge could be of help in interpreting the tendency for the abnormal-spectrum galaxies in distant clusters to be somewhat less centrally concentrated than the red, non-star-forming galaxies (Pickles & van der Kruit 1991; Gunn &

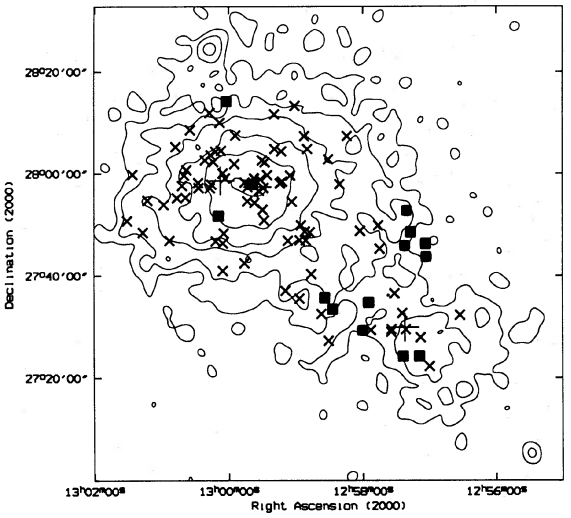

FIG. 16. The positions of all galaxies brighter than $B=17.2$ with Hydra observations are overlaid on the *ROSAT* x-ray map of Coma. Normal-spectrum galaxies are denoted by x's, abnormal-spectrum galaxies are denoted by filled squares, and the positions of a few bright galaxies (not observed with Hydra) are marked with plus signs for reference.

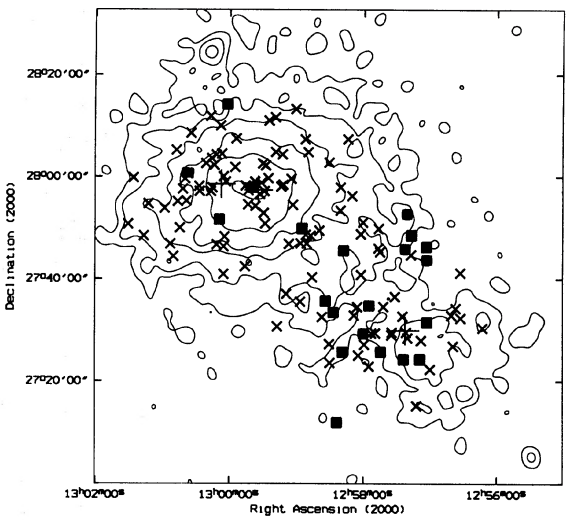

FIG. 17. Same as Fig. 16 except that *all* galaxies observed with Hydra are plotted.

Dressler 1988; Ellis 1988; Mellier *et al.* 1988). Allington-Smith *et al.* (1992) have shown that the radial distribution of blue galaxies in $B-O$ clusters is inconsistent with the specific model of Dressler & Gunn (1983) in which infalling gas-rich galaxies go through a starburst phase after encountering the hot intracluster medium, but the possibility remains that galaxy encounters with cluster gas could be a partial explanation for the starbursts, perhaps if the galaxies are all part of infalling groups. With that in mind, the recent *ROSAT* (Briel *et al.* 1992) and *Spacelab 2* (Watt *et al.* 1992) x-ray emission maps of the Coma cluster may be relevant. These studies have revealed a well-defined secondary peak in x-ray emission in the SW region of Coma that is close to the area of the abnormal-spectrum galaxies. In Fig. 16 we have overlaid the positions of our $B<17.2$ spectroscopic sample on a contour map of the *ROSAT* observations kindly provided by Briel. Filled circles denote the positions of the abnormal-spectrum galaxies, whereas the crosses denote the positions of galaxies with normal spectra. The positions of several prominent early-type galaxies (not observed by us) are also marked for reference.

As can be seen in Fig. 16, the abnormal-spectrum galaxies are concentrated in a region fairly close to the secondary x-ray peak. However, most of them actually lie *between* the peak and the cluster center. In Fig. 17 we have overlaid the positions of *all* galaxies observed with Hydra and have included six additional faint galaxies, for which we consider spectral abnormalities to be fairly well-established, among the abnormal-spectrum sample.

Other clues to the nature of the SW region have been noted by both Briel *et al.* and by Watt *et al.* There is a localized density enhancement in the galaxy distribution near the secondary x-ray peak (Mellier *et al.* 1988). The GMP catalogue, which forms the basis of our sample, also reveals the presence of this local enhancement in that the number density of galaxies in the SW field with $B<19$ is about twice that in the corresponding (unobserved) NE field. The cD galaxy NGC 4839 (Oemler 1976) resides in this local substructure in the galaxy distribution, and is one of only two reported cases of noncentrally located cD's [the other is NGC 6304 which Schombert (1987) also finds to be located in a subcluster within the Hercules cluster]. However, like the abnormal-spectrum galaxies, NGC 4839 lies closer to the center of Coma than does the secondary x-ray peak. Thus the existence of a spatially extended peak in the cluster x-ray emission in the SW region, the presence of a density enhancement in the vicinity, and the location of a cD galaxy in that enhancement all suggest the region contains a physical substructure within the larger cluster.

The positional offset between the x-ray peak and the galaxy substructure does suggest that some sort of a dynamical picture is required to explain the observations. Both Briel *et al.* (1992) and Watt *et al.* (1992) argue that a gravitationally bound substructure may be falling into Coma. If the substructure contains its own hot intracluster medium that is braked by its interaction with the hot medium in the main cluster, this would explain the separation between the galaxy substructure and the secondary x-ray peak.

The presence of so many abnormal galaxies on the leading side of this subclump suggests that their spectral abnormality might result directly from the ram-pressure associated with their infall. However, as we discuss below, a detailed consideration of the galaxies' velocities shows that the situation is not at all clear.

3.5 Radial Velocities in the SW Region

If the SW region represents a gravitationally bound infalling substructure, its velocity dispersion should be con-

siderably lower than that of the main cluster, as found by Dressler and Shectman (1988) for a sample of 15 clusters exhibiting substructure. Moreover, if the SW substructure can be considered as an independent cluster, it should obey the well-established relation between cluster x-ray luminosity and galaxy velocity dispersion of the form $L_x \sim \sigma^{\alpha}$, where α is typically found to be ~ 4 (Quintana & Melnick 1982). Given that estimates of the x-ray luminosity of the secondary peak by Briel *et al.* and by Watt *et al.* are no more than 6% of the main cluster, then one would expect the velocity dispersion of the SW region to be no more than half that of the main cluster, or ~ 500 km s^{-1}. As a comparison, A2197 and A262, two clusters with x-ray luminosities similar to that of the x-ray substructure in the SW of Coma, have velocity dispersions of 395 and 415 km s^{-1}, respectively, Quintana & Melnick (1982).

Using our velocity data, the mean velocity and velocity dispersion for the 73 galaxies in the central field are $V=6989$ km s^{-1} and $\sigma=1137^{+221}_{-159}$ km s^{-1}, where the superscripted and subscripted values represent the 95% confidence levels on σ. For the 60 galaxies in the SW field, $V=6864$ km s^{-1} and $\sigma=1016^{+223}_{-155}$ km s^{-1}. Inclusion of more galaxies from the ZCAT (Huchra 1993) gives similar results: The total number of galaxies with velocities in the central field rises to 260, yielding $V=7018$ km s^{-1} and $\sigma=1148$ km s^{-1}, while if the upper limit in velocity is set at 9500 km s^{-1} then we obtain $V=6888$ km s^{-1} and $\sigma=921$ km s^{-1} for 251 galaxies. For the SW field we obtain $V=6841$ km s^{-1} and $\sigma=963$ km s^{-1} for 84 galaxies (regardless of where the upper velocity cutoff is set). Hence at first glance, the velocity dispersions of the central and SW fields are indistinguishable to within the uncertainties. This is not the expected result if the SW region represents an infalling substructure, since, as mentioned above, one expects the smaller substructure to have a velocity dispersion of ~ 500 km s^{-1}. Even assuming that $\sim 50\%$ of the galaxies in this field belong to the main cluster, the velocity dispersion expected would be only $\sigma \sim 750$ km s^{-1}.

It is also interesting to compare the kinematics of the abnormal-spectrum galaxies to those of the normal galaxies, since such a comparison might offer clues to their relationship with the SW substructure. Taking the conservative approach of including only the eleven galaxies brighter than $B=17.2$ with CN/H8 < -0.5, as well as the three AGN galaxies, then the mean velocity and velocity dispersion for this group are 7162 km s^{-1} and 1381^{+856}_{-447} km s^{-1}, respectively. For the remaining 20 galaxies brighter than $B=17.2$ in the SW region, $V=6647$ km s^{-1} and $\sigma=759^{+349}_{-202}$ km s^{-1}. A Kolmogorov–Smirnov test rejects the hypothesis that the two samples are drawn from the sample population at the 3.4% significance level. If we consider *all* of the galaxies in the SW region, and include among the abnormal galaxies the 6 fainter galaxies for which we are reasonably confident that spectral abnormalities are present, then we find $V=7288$ km s^{-1} and $\sigma=1262^{+658}_{-348}$ km s^{-1} for the 17 abnormal galaxies, whereas $V=6696$ km s^{-1} and $\sigma=861^{+208}_{-68}$ km s^{-1} for the 43 normal-spectrum galaxies. The K–S test rejects the hypothesis that these two samples are drawn from the same population at the 0.5% significance level.

Two results emerge from this discussion. First, the velocity dispersion in the SW region appears to be inconsistent with that expected for the simple picture of a gravitationally bound infalling substructure. Second, the velocity dispersion of the abnormal-spectrum galaxies in the SW region appears to be higher than that for their normal counterparts in that area. This latter result makes it somewhat difficult to maintain that the abnormal-spectrum galaxies are all gravitationally bound members of the SW substructure, although larger dynamical samples are required to produce convincing conclusions. Additionally, since the E+A galaxies will have suffered star formation which produce their spectral signatures ~ 1 Gyr ago, a galaxy moving at a typical velocity of 1000 km s^{-1} would have traveled over 50′ in that time interval. Thus the presence of any spatial correlation with the x-ray emission is puzzling.

4. CONCLUSIONS

Multifiber spectroscopy of 125 early-type galaxies in two fields of the Coma cluster of galaxies has revealed that a surprising number of early-type galaxies in a field centered at $\approx 40'$ southwest of the cluster center, have spectra that reflect enhanced recent star formation activity and/or nuclear activity. These "abnormal" galaxies are found near a region of enhanced x-ray emission and of higher galaxy density than is characteristic of this radial zone. Our sample of galaxies reaches as faint as $B=19$ ($M_B=-15$), farther down the galaxy luminosity function than previously studied. The fraction of galaxies in this field affected by recent star formation appears to be approximately the same over the range of magnitudes studied.

The spectral peculiarities exhibited by the abnormal galaxies are quite distinct from those found in normal spirals, but are remarkably similar to those of the red Hδ-strong galaxies found by Couch & Sharples (1987) in several clusters at $z \approx 0.3$. We infer that, in Coma, we are witnessing the same kind of environmental effects on cluster galaxies that are commonly found in higher redshift systems.

Further detailed studies of the Coma cluster should provide us with a more comprehensive picture of environmental effects in clusters than can be obtained for their distant faint counterparts. The most pressing need is to extend the work we have presented here to study other regions surrounding the Coma cluster. It is important to determine whether the effect we are seeing is associated with the (possibly infalling) NGC 4839 group or whether such unusual galaxies form a shell surrounding an older core of galaxies at the center of the cluster.

The Coma galaxies and the associated x-ray gas can also be imaged at more than ten times higher spatial resolution than the more distant clusters. The proximity of Coma raises an important question with regard to the observations here, in that the star-formation activity we have observed is located in the nucleus, while the location of similar activity in more distant galaxies is at present uncertain. We have the opportunity in Coma of mapping in detail the

spatial distribution of star formation for comparison with data now being obtained for $z \simeq 0.3$–0.4 galaxies using the *Hubble Space Telescope*. The synthesis of these studies promises a unique advance in our understanding of evolutionary effects in clusters.

We wish to acknowledge Dr. Sam Barden and the Hydra team for producing such a superb multifiber instrument and for providing helpful support before and during the observing run. We also thank Dr. Rob Kennicutt for providing access to his catalog of spectra of nearby galaxies and Dr. Uli Briel for allowing us to use a digital contour map of the *ROSAT* all-sky PSPC image of Coma. J.A.R. acknowledges financial support from NSF Grant No. AST-8919455 to the University of North Carolina. R.S.E. and R.G.B. acknowledge financial support from the UK Science and Engineering Research Council.

APPENDIX A: DESCRIPTIONS OF INDIVIDUAL GALAXIES

We describe below the spectra of the individual abnormal galaxies shown in Fig. 2 in the context of the CCD images displayed in Fig. 9.

D15 is a Markarian object (MRK 55), previously studied by Sargent (1970) and others. It is an emission-line early-type galaxy (S0) and is the bluest galaxy we observed, but the absorption spectrum, to the extent that it can be discerned from under the intense emission spectrum, does not appear to be unusual. Because the Balmer emission lines are substantially narrower than the metallic forbidden lines, the D15 emission spectrum is probably the composite of a low-ionization nuclear emission region (LINER) and an H II region spectrum, with the forbidden lines dominated by the AGN phenomenon and the Balmer lines receiving a major contribution from H II regions. Specifically, the Hβ linewidth corresponds to 330 km s^{-1}, whereas the [O III]$\lambda\lambda$5007,4959 linewidths correspond to 500 km s^{-1}. To further study the nature of the emission spectrum, we use the (5007/4861) vs (3727/5007) diagnostic diagram of Baldwin *et al.* (1981, hereafter referred to as BPT). D15 has $\log(5007/4861) = -0.05$ and $\log(3727/5007) = 0.49$, which places it between the bulk of the LINER galaxies and the H II regions in Fig. 2 of BPT, which is entirely consistent with the idea that we are observing a composite between LINER and H II region spectra [Ne III]λ3869, which is commonly observed in LINER spectra, is also easily visible in the spectrum of D15. Data on emission lines are given in Table 2. Note that D15 has a companion galaxy in Fig. 9.

D45 has strong narrow emission lines (with typical linewidths corresponding to $\simeq$200 km s^{-1} FWHM) as well as an E+A absorption spectrum. Besides the strong E+A spectrum, D45 is unusual in that the emission is far too strong for its Hubble-type of Sa. Put another way, the equivalent width of 34 Å for 3727 is far too strong for its color, which is near the mean color for an E/S0 (for details, see discussion in Sec. *3.2.1* and Fig. 12). The galaxy has a small bulge, and a low surface brightness disk. The emission spectrum can be clearly seen in Fig. 18, where the spectrum of D45 has been divided by the combined spectra of three other Coma galaxies with enhanced Balmer lines, but no emission (D94, D112, and D99). The Balmer sequence is present as well as [O II]λ3727 and [O III]$\lambda\lambda$5007,4959. The emission-line intensity data are given in Table 2. We find that the low-excitation spectrum of D45 is dominated by an H II region spectrum for the following reasons. First, D45 lies exactly on the mean relation for the H II regions in the 5007/4861 vs 3727/5007 diagram of BPT's Fig. 2, with $\log(5007/4861) = -0.12$ and $\log(3727/4861) = 0.37$. Second, a recently acquired MMT spectrum in the red of D45 shows that Hα is much stronger than the [N II] lines at λ6584 and λ6548. In fact, the measured $\log(6584/6563) = -0.5$ definitely rules out the possibility that an AGN predominates the emission spectrum of D45 (see Fig. 5 of BPT).

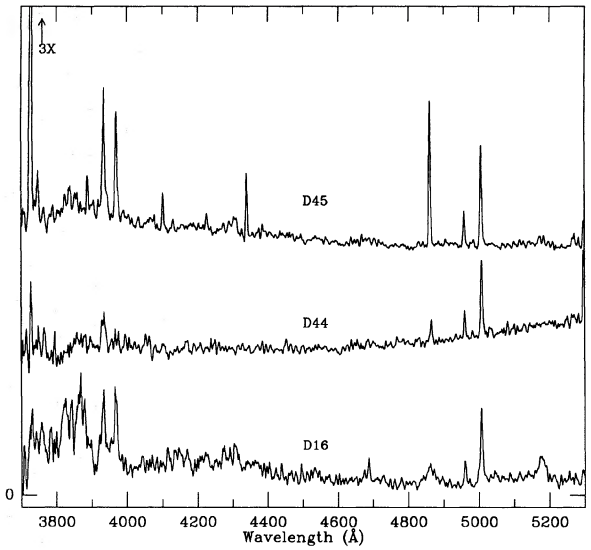

FIG. 18. (a) Spectrum of D45 divided by the composite spectrum of three Coma galaxies (D94, D112, and D99) having similar enhanced Balmer absorption, but no emission lines. (b) Spectrum of D44 divided by the same composite spectrum as in (a). (c) Spectrum of D16 divided by the composite spectrum of 70 normal-spectrum Coma galaxies.

D44 has both a fairly weak emission spectrum (with linewidths corresponding to $\simeq$300 km s^{-1}) and moderate E+A absorption. The emission spectrum can be easily seen in Fig. 18, where the spectrum of D44 has been divided by that of the same three E+A galaxies used in the case of D44 above. A spectrum in the red, recently acquired with the MMT, demonstrates convincingly that the emission spectrum in this galaxy is very similar to that of the nuclear region of M51 (see Rose & Searle 1982). Specifically, the [N II]/Hα ratio is extremely high ($\sim$5:1), too high for either an H II region spectrum or for a traditional LINER spectrum. When combined with the fairly high excitation of $\log(5007/4861) \sim 0.7$, the spectrum of D44 is seen to be almost identical to that of the nucleus of M51 [see Fig. 5 of Rose & Searle (1982)], i.e., intermediate in characteristics between a LINER and a Seyfert 2 (see Fig. 5 of BPT). In any case, the emission spectrum of D44

is dominated by an AGN, but a moderate E+A absorption spectrum is also present, making this galaxy unusual and perhaps unique in having both of these spectral abnormalities. The CCD image shows the galaxy to be an edge-on S0.

D16 has a particularly interesting weak emission spectrum and no evidence for enhanced Balmer absorption. As can be seen in Fig. 18, where the spectrum of D16 is divided by a composite of many normal Coma spectra, D16 has a very high-excitation narrow-line spectrum (the typical linewidth corresponding to $\approx$350 km s^{-1} FWHM). The spectrum has clearly too high an excitation to be that of a LINER. In fact, only an upper limit to the equivalent width of Hβ emission can be established, hence a lower limit to the excitation. We estimate an upper limit on Hβ of 0.45 A, which gives a lower limit on log(5007/4861) of 0.82. When combined with the log(3727/5007) = $-$0.54, we find that D16 occupies the area in Fig. 2 of BPT that is inhabited by Seyfert 2 spectra. The fact that He II 4686 emission can definitely be seen in Fig. 18, which is a line typically found only in gas photoionized by a relatively hard (e.g., power law) ionizing continuum, further establishes the Sy 2 nature of D16. A closer look at Fig. 18 also reveals that none of the major absorption lines in D16 are satisfactorily divided out by the composite normal Coma spectrum. All lines in D16, including Hβ, are weaker in D16 than in the composite spectrum, and so appear as "emission" features in the divided spectrum. Of course, the Hβ "emission" seen in Fig. 18 could in fact be a true broad-line Hβ from a Seyfert 1 spectrum, but the general weak-lined nature of D16 could be attributed to dilution from a nonstellar continuum. In either case, there may be evidence for a Sy 1 nature to D16 instead of a strictly Sy 2 spectrum. This interpretation has been confirmed through the recent acquisition of a spectrum in the red with the MMT. First, the ratio of [N II]λ6584 to Hα is high ($\sim$3:1), which definitely demonstrates that an AGN dominates the emission spectrum of D16. Furthermore, a broad-line component to Hα is evident in the red spectrum. The emission line profiles at [N II],Hα are very similar to those found for M81 by Peimbert & Torres-Peimbert (1981), as shown in their Fig. 2. As noted in Sec. 3.2.1, the low luminosity and weakness of the Seyfert spectrum in D16 makes it a highly unusual object. The galaxy itself is an S0, seen nearly face-on.

D43, first studied by Sparke *et al.* (1980) has an E+A absorption spectrum, plus weak emission of 3727, and possibly Hβ and O III. Sparke *et al.* did not report any emission (but their spectrum is redward of 3727 and their Hβ feature looks filled in with emission). It is the most luminous galaxy that we observed, and fairly blue. The galaxy appears to be an E from the CCD frame, though Dressler called it S0p.

GMP 4330 has moderate Balmer emission and fairly weak [O III]λ3727. A spectrum in the red, recently acquired with the MMT, reveals that Hα is much stronger than the [N II] lines [log(6584/6563) ~ -0.5]. The combination of low excitation and low [N II]/Hα demonstrates that the emission spectrum is dominated by H II regions.

D94 is a strong E+A absorption spectrum with no emission lines, and an S0, according to plates and the CCD frame.

D14 has no emission, a moderate E+A absorption spectrum. It is an edge-on S0.

D112 also has no emission, a moderate E+A absorption spectrum. The galaxy was called an E by Dressler and appears so on the CCD frame, although the 4 m classification was S0.

D99 has a strong E+A absorption spectrum, but no emission. It is the second bluest galaxy we observed, and is in the central field. Its eastern companion is D100, an irregular galaxy whose velocity is about 4700 km s^{-1} less than that of D99.

The next group consists of abnormal cases not as strong as those preceding.

D21 has strong H8 absorption, no emission.

D73 has a strong H8 line, and is an S0 as seen in Fig. 9.

D77 has a weak normal emission-line spectrum (actually only Hβ is seen, and a moderate E+A absorption-line spectrum. It is an edge-on S0.

D89 has a moderate E+A spectrum. This spectrum is highly vignetted (near the edge of the field). The galaxy is an edge-on S0, with a knot off nucleus, and perhaps a dust lane perpendicular to the disk (see Fig. 9). Its CN/H8 index is not quite extreme enough for it to be included among the abnormal-spectrum galaxies, but it is clear that the spectrum does exhibit enhanced Balmer lines indicative of recent star formation. It is in the middle of the central and SW fields; we arbitrarily placed it in the central field.

D216 has no emission, a moderate E+A absorption spectrum. This S0 is in the central field.

D127 has strong H8, but low S/N, in central field.

GMP 5100 has strong H8 (not shown in Fig. 2).

And finally, some marginal cases for which we have no images.

GMP 4294 has a strong H8 line.

D34 has a strong H8 line, also the H and K ratio is reversed.

D146 has strong H8 and Hδ, and is in the central field. The red color reported by GMP is not evident in the spectral energy distribution of this SB0/a (Fig. 2), thus its odd location in the color-magnitude diagram of Fig. 14 is probably incorrect.

APPENDIX B: BACKGROUND GALAXIES

The first three of these have similar redshifts, and thus are probably associated with each other.

D7 is an emission-line and E+A background galaxy (cz=20766.0$\pm$71 km s^{-1}). Interestingly, this object is an E galaxy (see Fig. 9), and thus is probably an example of a field or group elliptical undergoing star formation, consistent with its blue K-corrected ($B-V$)=0.52.

D55 is a normal E/S0 spectrum background galaxy (cz =20359$\pm$36 km s^{-1}).

GMP 4364 is a background galaxy (cz=20385$\pm$34

km s^{-1}) with weak [O II]λ3727 emission and enhanced H8 and Hδ. Hβ is partially filled in with emission.

GMP 4568 has strong emission lines and strong Balmer absorption. The redshift of 0.2671 ± 0.0002 requires a large K-correction to be made to its observed colors, resulting in a rest $B-V=-0.04$. This object is probably a distant spiral galaxy, though it is hard to tell from the CCD image (Fig. 9).

REFERENCES

Allington-Smith, J. R., Ellis, R. S., Zirbel, E. L., & Oemler, Jr., A. 1992, preprint

Baldwin, J. A., Phillips, M. M., & Terlevich, R. 1981, PASP, 93, 5 (BPT)

Bower, R. G., Ellis, R. S., Rose, J. A., & Sharples, R. M. 1990, AJ, 99, 530

Briel, U. G., Henry, J. P., & Bohringer, H. 1992, A&A, 259, L31

Burstein, D., Davies, R. L., Dressler, A., Faber, S. M., & Stone, R. P. S. 1987, ApJS, 64, 601

Butcher, H., & Oemler, A. 1978, ApJ, 219, 18

Butcher, H., & Oemler, A. 1984, ApJ, 285, 426

Caldwell, C. N. & Oemler, A. O. Jr. 1981, AJ, 86, 1424

Coleman, G. D., Wu C-C., & Weedman, D. W. 1980, ApJS, 43, 393

Couch, W. J., & Sharples, R. M. 1987, MNRAS, 229, 423 (CS)

Dressler, A. 1980a, ApJS, 42, 565

Dressler, A. 1980b, ApJ, 236, 351

Dressler, A. 1987, in Nearly Normal Galaxies, edited by S. M. Faber (Springer, New York), p. 276

Dressler, A., & Gunn, J. E. 1983, ApJ, 270, 7

Dressler, A., & Shectman, S. A. 1988, AJ, 95, 985

Ellis, R. S. 1988, in Towards an Understanding of Galaxies at High Redshift, edited by R. G. Kron and A. Renzini (Kluwer, Dordrecht), p. 147

Filippenko, A. V., & Sargent, W. L. W. 1989, ApJ, 342, L11

Godwin, J. G., Metcalfe, N., & Peach, J. V. 1983, MNRAS, 202, 113 (GMP)

Gunn, J. E., & Dressler, A. 1988, in Towards an Understanding of Galaxies at High Redshift, edited by R. G. Kron and A. Renzini (Kluwer, Dordrecht), p. 227

Huchra, J. P. 1993, CFA redshift catalog (unpublished)

Kennicutt, R. 1992a, ApJS, 79, 255

Kennicutt, R. 1992b, ApJ, 388, 310

Kunth, D., Sargent, W. L. W., & Bothun, G. D. 1987, AJ, 92, 29

Lavery, R. J., & Henry, J. P. 1986, ApJ, 304, L5

MacLaren, I., Ellis, R. S., & Couch, W. J. 1988, MNRAS, 230, 249

Mellier, Y., Soucail, G., Fort, B., & Mathez, G. 1988, A&A, 199, 13

Melnick, J., & Sargent, W. L. W. 1977, ApJ, 215, 401

Oemler, Jr., A. 1976, ApJ, 209, 693

Oemler, Jr., A. 1992, in Clusters and Superclusters of Galaxies, edited by A. C. Fabian (Kluwer, Dordrecht), p. 29

Osterbrock, D. E. 1974, Astrophysics of Gaseous Nebulae (W. H. Freeman, San Francisco)

Peimbert, M., & Torres-Peimbert, S. 1981, ApJ, 245, 845

Pence, W. D. 1976, ApJ, 203, 39

Pickles, A. J., & van der Kruit, P. C. 1991, A&AS, 91, 1

Quintana, H., & Melnick, J. 1982, AJ, 87, 972

Rose, J. A., & Searle, L. 1982, ApJ, 253, 556

Sargent, W. L. W. 1970, ApJ, 159, 765

Schombert, J. M. 1987, ApJS, 64, 643

Sparke, L. S., Kormendy, J., & Spinrad, H. 1980, ApJ, 235, 755

Watt, M. P., Ponman, T. J., Bertram, D., Eyles, C. J., Skinner, G. K., & Willmore, A. P. 1992, MNRAS, 258, 738

Whitmore, B. C., & Gilmore, D. M. 1991, ApJ, 367, 64

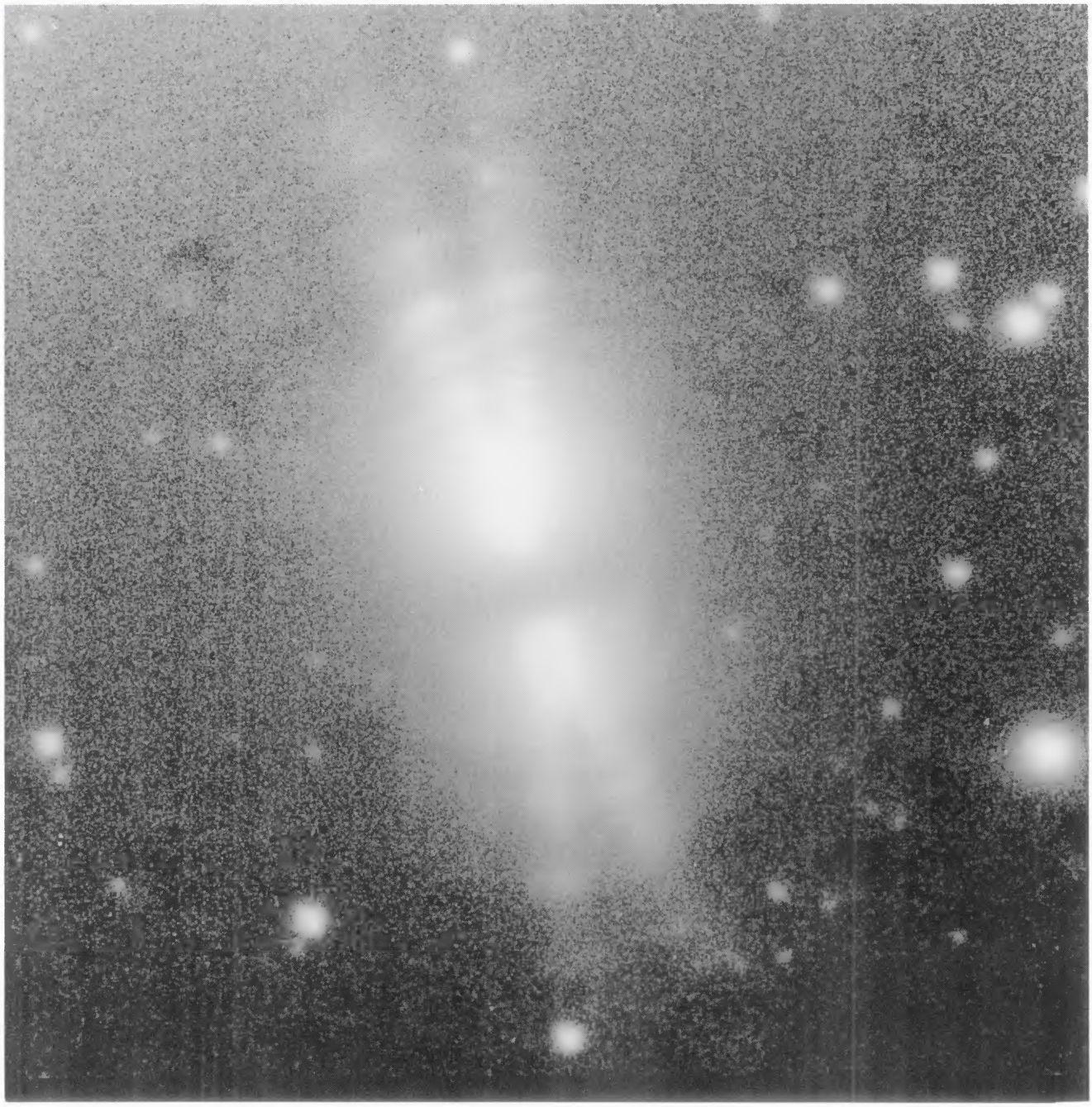

FIG. 1. Image of AFGL 2688 taken in the *I* band with the UH 1024×1024 CCD camera and 2.2 m telescope. The flux scale is logarithmic to show faint emission more clearly. Spatial scale is 52″ from top to bottom.

Latter *et al.* (see page 261)